Stable and Efficient Modeling of Anelastic Attenuation in Seismic Wave Propagation

N. Anders Petersson* and Björn Sjögreen

Center for Applied Scientific Computing, L-422, Lawrence Livermore National Laboratory, P.O. Box 808, Livermore, CA 94551, USA.

Abstract. We develop a stable finite difference approximation of the three-dimensional viscoelastic wave equation. The material model is a super-imposition of N standard linear solid mechanisms, which commonly is used in seismology to model a material with constant quality factor Q. The proposed scheme discretizes the governing equations in second order displacement formulation using $3N$ memory variables, making it significantly more memory efficient than the commonly used first order velocity-stress formulation. The new scheme is a generalization of our energy conserving finite difference scheme for the elastic wave equation in second order formulation [SIAM J. Numer. Anal., 45 (2007), pp. 1902–1936]. Our main result is a proof that the proposed discretization is energy stable, even in the case of variable material properties. The proof relies on the summation-by-parts property of the discretization. The new scheme is implemented with grid refinement with hanging nodes on the interface. Numerical experiments verify the accuracy and stability of the new scheme. Semi-analytical solutions for a half-space problem and the LOH.3 layer over half-space problem are used to demonstrate how the number of viscoelastic mechanisms and the grid resolution influence the accuracy. We find that three standard linear solid mechanisms usually are sufficient to make the modeling error smaller than the discretization error.

*Corresponding author. *Email addresses:* `andersp@llnl.gov` (N. A. Petersson), `sjogreen2@llnl.gov` (B. Sjögreen)

1   Introduction

Dissipative mechanisms in the earth lead to anelastic attenuation of seismic waves [1]. This attenuation is commonly modeled by describing the earth as a viscoelastic constant-Q absorption band solid, meaning that the material has a quality factor Q, which is independent of frequency. Such material behavior can be approximated in the time-domain by superimposing n standard linear solid (SLS) mechanisms [4].

In this article we develop a stable finite difference approximation of the three-dimensional viscoelastic wave equation with an n-SLS material model. The proposed scheme discretizes the governing equations in second order displacement formulation using $3n$ memory variables, making it significantly more memory efficient than the commonly used first order velocity-stress formulation. The discretization is a generalization of our summation-by-parts finite difference discretization of the elastic wave equation [19, 20, 22]. Our main result is a proof that the proposed discretization is energy stable, even in the case of variable material properties.

There is a substantial number of papers on anelastic attenuation in the literature on seismic wave propagation. Liu et al. [16] showed that the constant-Q material behavior can be approximated by superimposing n standard linear solid (SLS) mechanisms. Day and Minister [7] introduced a rational approximation of the viscoelastic modulus, which enabled realistic attenuation to be introduced in a time-domain seismic wave simulation. Emmerich and Korn [8] pointed out that the rational approximation of the viscoelastic modulus represents the rheological model of a generalized Maxwell body. They devised a least-squares technique of optimizing the coefficients in the rational approximation, which gave a significantly improved approximation of the constant-Q behavior. Moczo and Kristek [18] showed that the generalized Maxwell body used by Emmerich and Korn is equivalent to superimposing n SLS mechanisms. More recently, Savage et al. [23] found that a SLS with $n = 3$ mechanisms gives a close to constant Q-value over 1.7 decades in frequency, and illustrated how a higher number of mechanisms allows the frequency band to be made wider. Komatitisch et al. [13] and Käser et al. [12] reported very accurate results for the LOH.3 test problem [5], using three-dimensional time-domain simulations with $n = 3$ or $n = 4$ mechanisms. Bielak et al. [3] proposed a memory efficient approach based on the rheological model of a Kelvin-Voigt body in parallel with two Maxwell bodies, and reports an almost constant Q-value over two decades in frequency.

Large computational resources are often required for including realistic viscoelasticity in three-dimensional seismic wave simulations. The reason is that the n-SLS viscoelastic model requires a number of so called memory variables to be evolved together with the primary dependent variables (velocities and stresses, or displacements). Each memory variable adds an extra differential equation into the system that governs seismic wave propagation, and the numbers of extra variables and equations are proportional to n.

In the first order velocity-stress formulation, which commonly is used in seismic applications [10, 12, 15, 24], the isotropic elastic wave equation is a system of nine partial differential equations (PDEs) that govern the three components of the velocity and the

six unique components of the symmetric stress tensor. In this formulation, it is natural to introduce memory variables that express the viscoelastic contribution to the stress tensor. Each SLS in the viscoelastic model adds six PDEs and six memory variables to the system, resulting in a total of $9+6n$ equations [12]. Hence, even for the moderate value of $n=3$, the first order formulation leads to a system of 27 coupled PDEs. The isotropic elastic wave equation can also be written as a second order system, consisting of three PDEs governing the three components of the displacement (or the velocity). Also in this case can the viscoelastic model be formulated in terms of six memory variables per SLS [14]. However, based on the observation that only the divergence of the stress tensor is needed, we propose a more memory efficient approach where only three additional differential equations are added for each SLS. The total number of differential equations in the resulting system is $3+3n$, which is significantly less than the $9+6n$ equations for the first order formulation.

In addition to memory variables, there are extra material parameters in the viscoelastic model. The isotropic elastic wave equation has three material parameters: density and two Lamé parameters. The viscoelastic model adds two material parameters for each SLS. All these material parameters are field variables that may vary in space in a general way. The second order formulation uses the same number of material parameters as the first order velocity-stress approach. Emmerich and Korn's [8] procedure for determining these parameters has been used extensively in seismic applications [12, 15]. Liu and Archuleta [17] presented an alternative method for determining these parameters, based on interpolation. To save computational resources, some researchers [6, 10] have argued that the viscoelastic system could be reduced in size by placing the associated memory variables on alternating grid points in each direction of the three-dimensional computational grid. The memory requirement for such a coarse grained $n=8$ model would thus be the same as an $n=1$ model stored at every grid point. However, the accuracy of this approach is not well understood, especially when discontinuities are present in the material model [15]. Furthermore, it is not clear how to use the coarse graining technique when $n \neq 8$.

The reminder of the paper is organized as follows. After presenting the governing equations in Section 1.1, we derive an energy estimate for the continuous problem in Section 2, giving sufficient conditions on the material parameters for well-posedness of the viscoelastic wave equation. The spatial discretization is presented in Section 3, where the semi-discrete problem is shown to satisfy a corresponding energy estimate. In Section 4, we present a second order accurate explicit time discretization of the viscoelastic wave equation. We prove that this scheme is stable and satisfies an energy estimate under two conditions. First, the material parameters must satisfy the aforementioned conditions for well-posedness and, secondly, the time step must satisfy a CFL-type time step restriction. In Section 5 we outline Emmerich and Korn's [8] least squares method for determining the viscoelastic parameters. We evaluate the actual frequency dependence of Q for different number of mechanisms and widths of the frequency band. Three-dimensional numerical simulations are reported in Section 6, where we also outline how our scheme

can be generalized to a composite grid [22], with hanging nodes on the grid interface. Examples are given for the LOH.3 test case.

1.1 Viscoelastic modeling

The stress-strain relation in a linear viscoelastic material is defined by a convolution between stress relaxation functions and the time derivative of the strain, see e.g., [4]. Corresponding to the time-independent Lamé parameters for an elastic material, the two stress relaxation functions $\lambda(t)$ and $\mu(t)$ specify the stress tensor in an isotropic viscoelastic material,

$$\mathcal{T} = \int_{-\infty}^{t} \lambda(t-\tau)\frac{\partial \text{Tr}(\mathcal{D}(\mathbf{u}))(\tau)}{\partial \tau}Id\tau + \int_{-\infty}^{t} 2\mu(t-\tau)\frac{\partial \mathcal{D}(\mathbf{u})(\tau)}{\partial \tau}d\tau, \tag{1.1}$$

where I is the Kronecker delta. Let $\mathbf{u} = \mathbf{u}(\mathbf{x},t)$ be the displacement in the domain $\mathbf{x} \in \Omega \subset \mathbb{R}^3$. The strain tensor $\mathcal{D}$ is the symmetric part of the displacement gradient,

$$\mathcal{D}(\mathbf{u}) = \frac{1}{2}(\nabla\mathbf{u} + \nabla\mathbf{u}^T), \qquad \text{Tr}(\mathcal{D}(\mathbf{u})) \equiv \nabla\cdot\mathbf{u}.$$

We consider a material model obtained by superimposing n SLS mechanisms, leading to the stress-relaxation functions (see e.g., [4])

$$\mu(t) = H(t)\Big[\mu_0 - \sum_{\nu=1}^{n}\mu_\nu(1-e^{-\omega_\nu t})\Big], \qquad \lambda(t) = H(t)\Big[\lambda_0 - \sum_{\nu=1}^{n}\lambda_\nu(1-e^{-\omega_\nu t})\Big], \tag{1.2}$$

where $H(t)$ is the Heaviside step function, $\omega_\nu > 0$ are relaxation frequencies, and μ_ν and λ_ν are material parameters. After inserting (1.2) into (1.1) and integrating by parts in time, the stress tensor becomes

$$\mathcal{T} = \lambda_0(\nabla\cdot\mathbf{u})I + 2\mu_0\mathcal{D}(\mathbf{u}) - \int_{-\infty}^{t}\sum_{\nu=1}^{n}\omega_\nu\lambda_\nu e^{-\omega_\nu\tau}(\nabla\cdot\mathbf{u})Id\tau - 2\int_{-\infty}^{t}\sum_{\nu=1}^{n}\omega_\nu\mu_\nu e^{-\omega_\nu\tau}\mathcal{D}(\mathbf{u})d\tau.$$

There are several ways of introducing memory variables. In the second order formulation, only the divergence of the stress tensor is needed to evolve the displacement. As we shall see below, a memory efficient formulation is obtained by using the vector-valued memory variables

$$\bar{\mathbf{u}}^{(\nu)}(\mathbf{x},t) = \omega_\nu\int_{-\infty}^{t}\mathbf{u}(\mathbf{x},\tau)e^{-\omega_\nu(t-\tau)}d\tau. \tag{1.3}$$

In terms of these memory variables, the stress tensor can written as

$$\mathcal{T} = \lambda_0(\nabla\cdot\mathbf{u})I + 2\mu_0\mathcal{D}(\mathbf{u}) - \sum_{\nu=1}^{n}\Big[\lambda_\nu(\nabla\cdot\bar{\mathbf{u}}^{(\nu)})I + 2\mu_\nu\mathcal{D}(\bar{\mathbf{u}}^{(\nu)})\Big]. \tag{1.4}$$

The displacement is governed by Euler's equation for elasticity,

$$\rho\frac{\partial^2\mathbf{u}}{\partial t^2} = \nabla\cdot\mathcal{T} + \mathbf{F},$$

where ρ is the density of the material and $\mathbf{F}$ represents the external forcing. Evaluating the divergence of (1.4) gives,

$$\rho\frac{\partial^2\mathbf{u}}{\partial t^2}=\mathbf{L}(\lambda_0,\mu_0)\mathbf{u}-\sum_{\nu=1}^{n}\mathbf{L}(\lambda_\nu,\mu_\nu)\bar{\mathbf{u}}^{(\nu)}+\mathbf{F}, \qquad \mathbf{x}\in\Omega, \ \ t\geq0, \qquad (1.5a)$$

$$\mathbf{u}(\mathbf{x},0)=\mathbf{g}_0(\mathbf{x}), \qquad \mathbf{u}_t(\mathbf{x},0)=\mathbf{g}_1(\mathbf{x}), \qquad \mathbf{x}\in\Omega, \qquad (1.5b)$$

where $\mathbf{g}_0$, $\mathbf{g}_1$ are the initial data and the spatial operator is

$$\mathbf{L}(\lambda,\mu)\mathbf{u}=:\nabla(\lambda(\nabla\cdot\mathbf{u}))+\nabla\cdot(2\mu\mathcal{D}(\mathbf{u})). \qquad (1.6)$$

Appropriate boundary conditions for $\mathbf{u}$ will be discussed below.

We want to formulate an initial-value problem for the memory variables $\bar{\mathbf{u}}^{(\nu)}$. By splitting the time-integration in (1.3) over negative and positive times, we arrive at the modified formula,

$$\bar{\mathbf{u}}^{(\nu)}(\mathbf{x},t)=\bar{\mathbf{g}}^{(\nu)}(\mathbf{x})e^{-\omega_\nu t}+\omega_\nu\int_0^t\mathbf{u}(\mathbf{x},\tau)e^{-\omega_\nu(t-\tau)}d\tau, \qquad t\geq0, \qquad (1.7)$$

where

$$\bar{\mathbf{g}}^{(\nu)}(\mathbf{x})=\omega_\nu\int_{-\infty}^0\mathbf{u}(\mathbf{x},\tau)e^{\omega_\nu\tau}d\tau.$$

By differentiating (1.7) in time we find that the memory variables satisfy the differential equations

$$\frac{1}{\omega_\nu}\frac{\partial\bar{\mathbf{u}}^{(\nu)}}{\partial t}+\bar{\mathbf{u}}^{(\nu)}=\mathbf{u}, \qquad \mathbf{x}\in\Omega, \ \ t\geq0, \qquad (1.8a)$$

$$\bar{\mathbf{u}}^{(\nu)}(\mathbf{x},0)=\bar{\mathbf{g}}^{(\nu)}(\mathbf{x}), \qquad \mathbf{x}\in\Omega, \qquad (1.8b)$$

for $\nu=1,2,\cdots,n$. Note that $\bar{\mathbf{g}}^{(\nu)}(\mathbf{x})$ depends on the displacement history for $t<0$, which in many applications is unknown. It is therefore common to assume $\bar{\mathbf{g}}^{(\nu)}(\mathbf{x})=\mathbf{0}$, which corresponds to initially only using the purely elastic terms in (1.5). Non-zero initial conditions for $\bar{\mathbf{u}}^{(\nu)}$ are accommodated for by adding the solution of the homogeneous differential equation, i.e., $\bar{\mathbf{u}}_h^{(\nu)}=\bar{\mathbf{g}}^{(\nu)}e^{-\omega_\nu t}$. Thus, the influence of initial conditions on the memory variables decays exponentially fast in time.

The coupled system (1.5), (1.8) will in the following be referred to as the viscoelastic wave equation. There are three components in each of the vector variables $\mathbf{u}$ and $\bar{\mathbf{u}}^{(\nu)}$, $\nu=1,2,\cdots,n$, resulting in $3+3n$ differential equations for as many dependent variables. All spatial derivatives in the system occur in (1.5). Furthermore, note that each viscoelastic contributions to the right hand side of (1.5) is of the form $\mathbf{L}(\lambda_\nu,\mu_\nu)\bar{\mathbf{u}}^{(\nu)}$. This is the same spatial operator as in the purely elastic case, but with different material parameters and operating on $\bar{\mathbf{u}}^{(\nu)}$ instead of $\mathbf{u}$. Apart from being memory efficient, our formulation is therefore also straight forward to implement.

2   Energy estimate for the continuous viscoelastic wave equation

We define a scalar product for real-valued vector functions $\mathbf{u}(\mathbf{x}) = (u^1(\mathbf{x}), u^2(\mathbf{x}), u^3(\mathbf{x}))^T$ and $\mathbf{v}(\mathbf{x}) = (v^1(\mathbf{x}), v^2(\mathbf{x}), v^3(\mathbf{x}))^T$ in the bounded domain $\mathbf{x} \in \Omega$,

$$(\mathbf{u}, \mathbf{v}) = \int_\Omega \mathbf{u} \cdot \mathbf{v} \, d\Omega, \qquad \mathbf{u} \cdot \mathbf{v} = \sum_{j=1}^3 u^j v^j$$

with corresponding norm $\|\mathbf{u}\|^2 = (\mathbf{u}, \mathbf{u})$.

Gauss' theorem implies that the spatial operator $\mathbf{L}(\lambda_\nu, \mu_\nu)$ in (1.6) satisfies

$$\left(\mathbf{v}, \mathbf{L}(\lambda_\nu, \mu_\nu)\mathbf{u}\right) = \int_\Gamma \mathbf{v} \cdot \left[(\lambda_\nu \nabla \cdot \mathbf{u})\mathbf{n} + 2\mu_\nu \mathcal{D}(\mathbf{u})\mathbf{n}\right] d\Gamma - (\nabla \cdot \mathbf{v}, \lambda_\nu \nabla \cdot \mathbf{u})$$
$$- \int_\Omega 2\mu_\nu \mathcal{D}(\mathbf{v}) : \mathcal{D}(\mathbf{u}) \, d\Omega, \tag{2.1}$$

where Γ is the boundary of Ω with outwardly directed unit normal $\mathbf{n}$. The contraction between two tensors with Cartesian components A_{ij} and B_{ij} is defined by $A : B = \sum_{i=1}^3 \sum_{j=1}^3 A_{ij} B_{ij}$.

The identity (2.1) has the structure

$$(\mathbf{v}, \mathbf{L}(\lambda_\nu, \mu_\nu)\mathbf{u}) = -S_\nu(\mathbf{v}, \mathbf{u}) + B_\nu(\mathbf{v}, \mathbf{u}), \tag{2.2}$$

where $S_\nu(\mathbf{v}, \mathbf{u})$ and $B_\nu(\mathbf{v}, \mathbf{u})$ denote the interior and boundary terms, respectively,

$$S_\nu(\mathbf{v}, \mathbf{u}) = (\nabla \cdot \mathbf{v}, \lambda_\nu \nabla \cdot \mathbf{u}) + \int_\Omega 2\mu_\nu \mathcal{D}(\mathbf{v}) : \mathcal{D}(\mathbf{u}) \, d\Omega, \tag{2.3a}$$

$$B_\nu(\mathbf{v}, \mathbf{u}) = \int_\Gamma \mathbf{v} \cdot \left[(\lambda_\nu \nabla \cdot \mathbf{u})\mathbf{n} + 2\mu_\nu \mathcal{D}(\mathbf{u})\mathbf{n}\right] d\Gamma. \tag{2.3b}$$

It follows by inspection of (2.3a) that each function $S_\nu(\mathbf{u}, \mathbf{v})$ is symmetric and bi-linear. Because $S_\nu(\mathbf{u}, \mathbf{u})$ is an integral over quadratic terms, it is non-negative if $\mu_\nu(\mathbf{x}) > 0$ and $\lambda_\nu(\mathbf{x}) > 0$.

It is well known that the spatial operator $L(\lambda_\nu, \mu_\nu)\mathbf{u} = 0$ for all $\mathbf{u} \in \mathbb{U}$, where $\mathbb{U}$ is the six-dimensional subspace corresponding to rigid body motions. The null-space $\mathbb{U}$ is spanned by three translational and three rotational basis functions. Since the boundary term (2.3b) is zero for all $\mathbf{u} \in \mathbb{U}$, we have $S_\nu(\mathbf{u}, \mathbf{u}) = 0$ for all $\mathbf{u} \in \mathbb{U}$. It is straight forward to show that, for sufficiently regular $\mathbf{u}$, there are no additional non-trivial solutions of $S_\nu(\mathbf{u}, \mathbf{u}) = 0$.

We consider two boundary conditions for (1.5), (1.8). First, the Dirichlet condition

$$\mathbf{u}(\mathbf{x}, t) = 0, \quad \mathbf{x} \in \Gamma, \quad t \geq 0. \tag{2.4}$$

The second type of boundary condition is the traction-free condition $\mathcal{T}\mathbf{n} = 0$ imposed on the viscoelastic stress tensor (1.4),

$$(\lambda_0 \nabla \cdot \mathbf{u})\mathbf{n} + 2\mu_0 \mathcal{D}(\mathbf{u})\mathbf{n} = \sum_{\nu=1}^n (\lambda_\nu \nabla \cdot \bar{\mathbf{u}}^{(\nu)})\mathbf{n} + 2\mu_\nu \mathcal{D}(\bar{\mathbf{u}}^{(\nu)})\mathbf{n}, \quad \mathbf{x} \in \Gamma, \quad t \geq 0. \tag{2.5}$$

On a free surface boundary, (2.5) is the physically correct boundary condition because it sets the normal component of the viscoelastic stress tensor to zero. Note that no explicit boundary condition is needed for the memory variables in (2.4) or (2.5), because they are solutions of the ordinary differential equations (1.8) on the boundary.

Define the viscoelastic energy according to

$$e(t) = \|\sqrt{\rho}\mathbf{u}_t\|^2 + S_0(\mathbf{u},\mathbf{u}) - \sum_{\nu=1}^{n} S_\nu(\mathbf{u},\mathbf{u}) + \sum_{\nu=1}^{n} S_\nu(\mathbf{u}-\bar{\mathbf{u}}^{(\nu)},\mathbf{u}-\bar{\mathbf{u}}^{(\nu)}). \tag{2.6}$$

Our first main result, stated below, provides sufficient conditions on the material properties for making the viscoelastic wave equation a well-posed problem in the energy seminorm.

Theorem 2.1. *Assume that the material data satisfy*

$$\lambda_0 - \sum_{\nu=1}^{n} \lambda_\nu \geq \tilde{\lambda}_{\min} > 0, \qquad \mu_0 - \sum_{\nu=1}^{n} \mu_\nu \geq \tilde{\mu}_{\min} > 0, \tag{2.7}$$

and

$$\rho \geq \rho_{\min} > 0, \quad \lambda_\nu \geq \lambda_{\min} > 0, \quad \mu_\nu \geq \mu_{\min} > 0, \quad \nu = 1, \cdots, n. \tag{2.8}$$

Then the solution of the viscoelastic wave equation (1.5), (1.8), *with* $\mathbf{F} = 0$, *subject to either the boundary condition* (2.4), *or* (2.5), *has non-increasing energy,*

$$e(t) \leq e(0), \quad t \geq 0. \tag{2.9}$$

Furthermore, $e(t)$ can be bounded from below according to

$$\rho_{\min}\|\mathbf{u}_t(\cdot,t)\|^2 + 2\tilde{\mu}_{\min}\|\mathcal{D}(\mathbf{u})(\cdot,t)\|^2 + \tilde{\lambda}_{\min}\|\nabla\cdot\mathbf{u}(\cdot,t)\|^2 \leq e(t). \tag{2.10}$$

Here, we define the norm of the tensor function $\mathcal{D}(\mathbf{u})$ by $\|\mathcal{D}\|^2 = \int_\Omega \mathcal{D}:\mathcal{D}d\Omega$.

Proof. The non-increasing energy follows from the identity

$$\frac{1}{2}\frac{de}{dt} = B_0(\mathbf{u}_t,\mathbf{u}) - \sum_{\nu=1}^{n} B_\nu(\mathbf{u}_t,\bar{\mathbf{u}}^{(\nu)}) - \sum_{\nu=1}^{n} \frac{1}{\omega_\nu} S_\nu(\bar{\mathbf{u}}_t^{(\nu)},\bar{\mathbf{u}}_t^{(\nu)}) \tag{2.11}$$

together with $S_\nu(\bar{\mathbf{u}}^{(\nu)},\bar{\mathbf{u}}^{(\nu)}) \geq 0$, and the fact that either one of the boundary conditions (2.4)-(2.5) make the boundary term $B_0 - \sum_{\nu=1}^{n} B_\nu$ equal to zero. Hence, $de/dt \leq 0$, which shows (2.9).

To prove identity (2.11), multiply (1.5) by $\mathbf{u}_t$ and integrate over Ω,

$$\frac{1}{2}\frac{d}{dt}(\mathbf{u}_t,\rho\mathbf{u}_t) = (\mathbf{u}_t,\rho\mathbf{u}_{tt}) = (\mathbf{u}_t,\mathbf{L}(\lambda_0,\mu_0)\mathbf{u}) - \sum_{\nu=1}^{n}(\mathbf{u}_t,\mathbf{L}(\lambda_\nu,\mu_\nu)\bar{\mathbf{u}}^{(\nu)})$$

$$= -S_0(\mathbf{u}_t,\mathbf{u}) + B_0(\mathbf{u}_t,\mathbf{u}) + \sum_{\nu=1}^{n} S_\nu(\mathbf{u}_t,\bar{\mathbf{u}}^{(\nu)}) - \sum_{\nu=1}^{n} B_\nu(\mathbf{u}_t,\bar{\mathbf{u}}^{(\nu)}). \tag{2.12}$$

The symmetry and bi-linear properties of S_ν show that

$$S_0(\mathbf{u}_t,\mathbf{u}) = \frac{1}{2}\frac{d}{dt}S_0(\mathbf{u},\mathbf{u}), \tag{2.13a}$$

$$S_\nu(\mathbf{u}_t,\bar{\mathbf{u}}^{(\nu)}) = \frac{d}{dt}S_\nu(\mathbf{u},\bar{\mathbf{u}}^{(\nu)}) - S_\nu(\mathbf{u},\bar{\mathbf{u}}_t^{(\nu)}). \tag{2.13b}$$

Furthermore, (1.8) gives

$$S_\nu(\mathbf{u},\bar{\mathbf{u}}_t^{(\nu)}) = \frac{1}{2}\frac{d}{dt}S_\nu(\bar{\mathbf{u}}^{(\nu)},\bar{\mathbf{u}}^{(\nu)}) + \frac{1}{\omega_\nu}S_\nu(\bar{\mathbf{u}}_t^{(\nu)},\bar{\mathbf{u}}_t^{(\nu)}),$$

which, substituted for the last term in (2.13b), leads to

$$S_\nu(\mathbf{u}_t,\bar{\mathbf{u}}^{(\nu)}) = \frac{1}{2}\frac{d}{dt}\left(2S_\nu(\mathbf{u},\bar{\mathbf{u}}^{(\nu)}) - S_\nu(\bar{\mathbf{u}}^{(\nu)},\bar{\mathbf{u}}^{(\nu)})\right) - \frac{1}{\omega_\nu}S_\nu(\bar{\mathbf{u}}_t^{(\nu)},\bar{\mathbf{u}}_t^{(\nu)}). \tag{2.14}$$

Finally, the identity

$$S_\nu(\mathbf{u}-\bar{\mathbf{u}}^{(\nu)},\mathbf{u}-\bar{\mathbf{u}}^{(\nu)}) = S_\nu(\mathbf{u},\mathbf{u}) - 2S_\nu(\mathbf{u},\bar{\mathbf{u}}^{(\nu)}) + S_\nu(\bar{\mathbf{u}}^{(\nu)},\bar{\mathbf{u}}^{(\nu)})$$

makes it possible to rewrite (2.14) as

$$S_\nu(\mathbf{u}_t,\bar{\mathbf{u}}^{(\nu)}) = \frac{1}{2}\frac{d}{dt}\left(S_\nu(\mathbf{u},\mathbf{u}) - S_\nu(\mathbf{u}-\bar{\mathbf{u}}^{(\nu)},\mathbf{u}-\bar{\mathbf{u}}^{(\nu)})\right) - \frac{1}{\omega_\nu}S_\nu(\bar{\mathbf{u}}_t^{(\nu)},\bar{\mathbf{u}}_t^{(\nu)}). \tag{2.15}$$

Relations (2.13a) and (2.15) give

$$-S_0(\mathbf{u}_t,\mathbf{u}) + \sum_{\nu=1}^{n}S_\nu(\mathbf{u}_t,\bar{\mathbf{u}}^{(\nu)})$$

$$= -\sum_{\nu=1}^{n}\frac{1}{\omega_\nu}S_\nu(\bar{\mathbf{u}}_t^{(\nu)},\bar{\mathbf{u}}_t^{(\nu)}) - \frac{1}{2}\frac{d}{dt}\left[S_0(\mathbf{u},\mathbf{u}) + \sum_{\nu=1}^{n}S_\nu(\mathbf{u}-\bar{\mathbf{u}}^{(\nu)},\mathbf{u}-\bar{\mathbf{u}}^{(\nu)}) - \sum_{\nu=1}^{n}S_\nu(\mathbf{u},\mathbf{u})\right],$$

which inserted into (2.12) yields the identity (2.11).

It remains to prove that the energy can be bounded from below. Inspection of (2.3a) shows that

$$S_0(\mathbf{u},\mathbf{u}) - \sum_{\nu=1}^{n}S_\nu(\mathbf{u},\mathbf{u}) = (\nabla\cdot\mathbf{u},\tilde{\lambda}\nabla\cdot\mathbf{u}) + \int_\Omega 2\tilde{\mu}\mathcal{D}(\mathbf{u}):\mathcal{D}(\mathbf{u})d\Omega,$$

$$\tilde{\lambda} = \lambda_0 - \sum_{\nu=1}^{n}\lambda_\nu, \qquad \tilde{\mu} = \mu_0 - \sum_{\nu=1}^{n}\mu_\nu. \tag{2.16}$$

Hence, if (2.7) is satisfied, $\tilde{\lambda} \geq \tilde{\lambda}_{\min} > 0$ and $\tilde{\mu} \geq \tilde{\mu}_{\min} > 0$, so

$$S_0(\mathbf{u},\mathbf{u}) - \sum_{\nu=1}^{n}S_\nu(\mathbf{u},\mathbf{u}) = \left\|\sqrt{\tilde{\lambda}}\nabla\cdot\mathbf{u}\right\|^2 + \left\|\sqrt{2\tilde{\mu}}\mathcal{D}(\mathbf{u})\right\|^2.$$

Because of material condition (2.8), the terms $S_\nu(\mathbf{u}-\bar{\mathbf{u}}^{(\nu)},\mathbf{u}-\bar{\mathbf{u}}^{(\nu)})$ in (2.6) are non-negative and do not have to be bounded further. Furthermore, assumption (2.7) gives $\tilde{\lambda} \geq \tilde{\lambda}_{\min}$, $\tilde{\mu} \geq \tilde{\mu}_{\min}$, which together with $\rho \geq \rho_{\min}$ proves (2.10). $\qquad\square$

Remark 2.1. If $\mathbf{u}$ is a solution of the viscoelastic wave equation subject to the Dirichlet boundary condition (2.4), there can be no rigid body motion component in $\mathbf{u}$. Korn's inequality [11] can then be used to bound the spatial derivatives in $e(t)$, leading to

$$c\left(\|\mathbf{u}_t\|^2 + \|\nabla \mathbf{u}\|^2 + \|\mathbf{u}\|^2\right) \leq e, \qquad c = \text{const.}$$

Remark 2.2. The conditions on λ_ν for bounding the spatial operator in $e(t)$ can be relaxed to

$$3\tilde{\lambda} + 2\tilde{\mu} \geq \epsilon > 0, \qquad 3\lambda_\nu + 2\mu_\nu \geq \epsilon > 0, \qquad \nu = 0, 1, \cdots, n,$$

where ϵ is a constant. The above conditions guarantee that the bulk modulus, $\lambda + 2\mu/3$, is positive.

3 The spatially discretized problem

We discretize the viscoelastic wave equation on the domain $0 \leq x \leq a$, $0 \leq y \leq b$, $0 \leq z \leq c$. We use a grid size $h > 0$ and define a grid by $x_i = (i-1)h$, $y_j = (j-1)h$, $z_k = (k-1)h$, with $0 \leq i \leq N_x + 1$, $0 \leq j \leq N_y + 1$, $0 \leq k \leq N_z + 1$. The domain sizes and the grid spacing are defined such that $x_{N_x} = a$, $y_{N_y} = b$, and $z_{N_z} = c$. The points outside the domain ($i = 0$, $i = N_x + 1$, $j = 0$, $j = N_y + 1$, $k = 0$, and $k = N_z + 1$) are ghost points, which are used to simplify the discretization of the boundary conditions. A scalar grid function is denoted $u_{i,j,k} = u(x_i, y_j, z_k)$ and $\mathbf{u}_{i,j,k}$ is a vector valued grid function.

The spatial discretization is based on our energy conserving method for the elastic wave equation [19, 20, 22]. While the ordinary differential equations (1.8) simply are enforced at each grid point in space, the semi-discrete problem corresponding to (1.5) is given by

$$\rho_{i,j,k} \frac{d^2 \mathbf{u}_{i,j,k}}{dt^2} = \mathbf{L}_h(\lambda_0, \mu_0) \mathbf{u}_{i,j,k} - \sum_{\nu=1}^{n} \mathbf{L}_h(\lambda_\nu, \mu_\nu) \bar{\mathbf{u}}_{i,j,k}^{(\nu)} + \mathbf{F}_{i,j,k}, \tag{3.1a}$$

$$\mathbf{u}_{i,j,k}(0) = \mathbf{f}_0(\mathbf{x}_{i,j,k}), \qquad (\mathbf{u}_t)_{i,j,k}(0) = \mathbf{f}_1(\mathbf{x}_{i,j,k}), \tag{3.1b}$$

for $1 \leq i \leq N_x$, $1 \leq j \leq N_y$, $1 \leq k \leq N_z$, where $\mathbf{L}_h(\lambda, \mu) \mathbf{u}_{i,j,k}$ is the discretization of the continuous operator (1.6). In component form,

$$\mathbf{L}_h(\lambda, \mu) \mathbf{u} = \left(L_h^{(1)}(\lambda, \mu) \mathbf{u}, L_h^{(2)}(\lambda, \mu) \mathbf{u}, L_h^{(3)}(\lambda, \mu) \mathbf{u}\right)^T,$$

where

$$L_h^{(1)}(\lambda, \mu) \mathbf{u} = D_-^x \left(E_{\frac{1}{2}}^x (2\mu + \lambda) D_+^x u^1\right) + D_-^y \left(E_{\frac{1}{2}}^y (\mu) D_+^y u^1\right) + D_-^z \left(E_{\frac{1}{2}}^z (\mu) D_+^z u^1\right)$$
$$+ \widetilde{D_0^x} \left(\lambda \widetilde{D_0^y} u^2 + \lambda \widetilde{D_0^z} u^3\right) + \widetilde{D_0^y} \left(\mu \widetilde{D_0^x} u^2\right) + \widetilde{D_0^z} \left(\mu \widetilde{D_0^x} u^3\right), \tag{3.2a}$$

$$L_h^{(2)}(\lambda,\mu)\mathbf{u} = D_-^x\left(E_{\frac{1}{2}}^x(\mu)D_+^x u^2\right) + D_-^y\left(E_{\frac{1}{2}}^y(2\mu+\lambda)D_+^y u^2\right) + D_-^z\left(E_{\frac{1}{2}}^z(\mu)D_+^z u^2\right)$$
$$+ \widetilde{D_0^x}(\mu\widetilde{D_0^y}u^1) + \widetilde{D_0^y}(\lambda\widetilde{D_0^x}u^1 + \lambda\widetilde{D_0^z}u^3) + \widetilde{D_0^z}(\mu\widetilde{D_0^y}u^3), \tag{3.2b}$$

$$L_h^{(3)}(\lambda,\mu)\mathbf{u} = D_-^x\left(E_{\frac{1}{2}}^x(\mu)D_+^x u^3\right) + D_-^y\left(E_{\frac{1}{2}}^y(\mu)D_+^y u^3\right) + D_-^z\left(E_{\frac{1}{2}}^z(2\mu+\lambda)D_+^z u^3\right)$$
$$+ \widetilde{D_0^x}(\mu\widetilde{D_0^z}u^1) + \widetilde{D_0^y}(\mu\widetilde{D_0^z}u^2) + \widetilde{D_0^z}(\lambda\widetilde{D_0^x}u^1 + \lambda\widetilde{D_0^y}u^2). \tag{3.2c}$$

Similar to the continuous case we denote the components of $\mathbf{u}$ by (u^1, u^2, u^3), and use a multi-dimensional notation of the standard divided difference operators, i.e.,

$$D_+^x u_{i,j,k} = \frac{(u_{i+1,j,k} - u_{i,j,k})}{h}, \qquad D_-^x u_{i,j,k} = D_+^x u_{i-1,j,k}, \qquad D_0^x = \frac{1}{2}(D_+^x + D_-^x).$$

The boundary modified operator for differences in the x-direction is defined by

$$\widetilde{D_0^x}u_{i,j,k} = \begin{cases} D_+^x u_{i,j,k}, & i=1, \\ D_0^x u_{i,j,k}, & 2 \le i \le N_x - 1, \\ D_-^x u_{i,j,k}, & i = N_x, \end{cases}$$

and the multi-dimensional averaging operator is defined by

$$E_{\frac{1}{2}}^x(\mu)_{i,j,k} = \frac{(\mu_{i+1,j,k} + \mu_{i,j,k})}{2}.$$

The superscripts on the difference and averaging operators denote the direction in which the operator is applied and we use corresponding definitions for the difference operators in the y- and z-directions.

We introduce a discrete scalar product for real-valued vector grid functions,

$$(\mathbf{u},\mathbf{v})_h = h^3 \sum_{i=1}^{N_x} \sum_{j=1}^{N_y} \sum_{k=1}^{N_z} a_i^{(x)} a_j^{(y)} a_k^{(z)} \mathbf{u}_{i,j,k} \cdot \mathbf{v}_{i,j,k},$$

where the weights satisfy

$$a_i^{(x)} = \begin{cases} \dfrac{1}{2}, & i=1 \text{ or } i=N_x, \\ 1, & 2 \le i \le N_x - 1, \end{cases}$$

with corresponding definitions of $a^{(y)}$ and $a^{(z)}$. The discrete norm is defined by $\|\mathbf{u}\|_h^2 = (\mathbf{u},\mathbf{u})_h$.

The spatial discretization satisfies a summation by parts principle corresponding to the integration by parts relation (2.2). In [20] (Lemma 3.1), it is proven that

$$(\mathbf{v}, \mathbf{L}_h(\lambda_\nu, \mu_\nu)\mathbf{u})_h = -S_\nu^{(h)}(\mathbf{v}, \mathbf{u}) + B_\nu^{(h)}(\mathbf{v}, \mathbf{u}). \tag{3.3}$$

The expression for the interior term $S_\nu^{(h)}$ is given in Appendix A. As in the continuous case, $S_\nu^{(h)}(\mathbf{v},\mathbf{u}) = S_\nu^{(h)}(\mathbf{u},\mathbf{v})$. The expression for $S_\nu^{(h)}(\mathbf{u},\mathbf{u})$ consists of a sum of quadratic terms and, if $\lambda_\nu \geq \lambda_{\min} > 0$ and $\mu_\nu \geq \mu_{\min} > 0$, it is positive semi-definite. In Appendix B we show that the null space of $S_\nu^{(h)}(\mathbf{u},\mathbf{u})$ is six-dimensional and corresponds to the same rigid body motions as in the continuous case.

The non-symmetric boundary term $B_\nu^{(h)}(\mathbf{u},\mathbf{v})$ was derived in the context of the elastic wave equation in [20]. Here we restate the result to explain how to impose boundary conditions for the viscoelastic case,

$$
\begin{aligned}
B_\nu^{(h)}(\mathbf{u},\mathbf{v}) = & h^2 \sum_{j=1}^{N_y} \sum_{k=1}^{N_z} a_j^{(y)} a_k^{(z)} \left(-\mathbf{u}_{1,j,k} \cdot \mathbf{B}_\nu^{(h)}(\mathbf{v})_{1,j,k}^{(x)} + \mathbf{u}_{N_x,j,k} \cdot \mathbf{B}_\nu^{(h)}(\mathbf{v})_{N_x,j,k}^{(x)} \right) \\
& + h^2 \sum_{i=1}^{N_x} \sum_{k=1}^{N_z} a_i^{(x)} a_k^{(z)} \left(-\mathbf{u}_{i,1,k} \cdot \mathbf{B}_\nu^{(h)}(\mathbf{v})_{i,1,k}^{(y)} + \mathbf{u}_{i,N_y,k} \cdot \mathbf{B}_\nu^{(h)}(\mathbf{v})_{i,N_y,k}^{(y)} \right) \\
& + h^2 \sum_{i=1}^{N_x} \sum_{j=1}^{N_y} a_i^{(x)} a_j^{(y)} \left(-\mathbf{u}_{i,j,1} \cdot \mathbf{B}_\nu^{(h)}(\mathbf{v})_{i,j,1}^{(z)} + \mathbf{u}_{i,j,N_z} \cdot \mathbf{B}_\nu^{(h)}(\mathbf{v})_{i,j,N_z}^{(z)} \right).
\end{aligned}
\tag{3.4}
$$

In the above expression, $\mathbf{B}_\nu^{(x)}$, $\mathbf{B}_\nu^{(y)}$, and $\mathbf{B}_\nu^{(z)}$ denote the discretized boundary stresses normal to the x, y, and z-directions, respectively. The discretization of the normal stresses is given by the boundary terms that emerges in identity (3.3), as described in [20]. For example, the discretized boundary stress in the z-direction on $k=1$ or $k=N_z$ is

$$
\mathbf{B}_\nu^{(h)}(\mathbf{u})_{i,j,k}^{(z)} = \begin{pmatrix}
\frac{1}{2}\mu_{i,j,k-\frac{1}{2}}^{(\nu)} D_-^z u_{i,j,k} + \frac{1}{2}\mu_{i,j,k+\frac{1}{2}}^{(\nu)} D_+^z u_{i,j,k} + \mu_{i,j,k}^{(\nu)} \widetilde{D_0^x} w_{i,j,k} \\
\frac{1}{2}\mu_{i,j,k-\frac{1}{2}}^{(\nu)} D_-^z v_{i,j,k} + \frac{1}{2}\mu_{i,j,k+\frac{1}{2}}^{(\nu)} D_+^z v_{i,j,k} + \mu_{i,j,k}^{(\nu)} \widetilde{D_0^y} w_{i,j,k} \\
\frac{1}{2}(2\mu^{(\nu)}+\lambda^{(\nu)})_{i,j,k-\frac{1}{2}} D_-^z w_{i,j,k} + \frac{1}{2}(2\mu^{(\nu)}+\lambda^{(\nu)})_{i,j,k+\frac{1}{2}} D_+^z w_{i,j,k} \\
+ \lambda_{i,j,k}^{(\nu)} (\widetilde{D_0^x} u_{i,j,k} + \widetilde{D_0^y} v_{i,j,k})
\end{pmatrix}.
\tag{3.5}
$$

Here, $\mu_{i,j,k+1/2}^{(\nu)} = E_{1/2}^z (\mu^{(\nu)})_{i,j,k}$, and the grid point values of the material parameters are defined by $\mu_{i,j,k}^{(\nu)} = \mu_\nu(\mathbf{x}_{i,j,k})$, with a similar definition of $\lambda_{i,j,k}^{(\nu)}$.

To simplify the presentation we only describe the boundary conditions along the boundary $k=N_z$; the other boundaries are treated in a corresponding way. The Dirichlet boundary condition (2.4) is enforced by setting

$$
\mathbf{u}_{i,j,N_z} = 0, \quad 1 \leq i \leq N_x, \quad 1 \leq j \leq N_y, \quad t \geq 0,
\tag{3.6}
$$

and the discretized version of the free surface boundary condition (2.5) is

$$
\mathbf{B}_0^{(h)}(\mathbf{u})_{i,j,N_z}^{(z)} = \sum_{\nu=1}^{n} \mathbf{B}_\nu^{(h)}(\bar{\mathbf{u}}^{(\nu)})_{i,j,N_z}^{(z)}, \quad 1 \leq i \leq N_x, \quad 1 \leq j \leq N_y, \quad t \geq 0.
\tag{3.7}
$$

Because the discretized problem satisfies identity (3.3), $S_\nu^{(h)}$ is positive semi-definite, and (3.6) or (3.7) will eliminate contributions from $B_\nu^{(h)}$ terms, we can derive an energy estimate corresponding to Theorem 2.1 in exactly the same way as in the continuous case. The resulting estimate follows by replacing the continuous scalar product by $(\cdot,\cdot)_h$, replacing S_ν by $S_\nu^{(h)}$, and B_ν by $B_\nu^{(h)}$. However, the lower bound of the energy needs to be modified because of the spatial discretization. This is discussed in more detail in the following section.

4   Time discretization

We discretize time on a uniform grid $t_m = m\Delta t$ with step size $\Delta t > 0$, and use the notation $\mathbf{u}_{i,j,k}^m$ for the approximation of $\mathbf{u}_{i,j,k}(t_m)$. For the elastic wave equation, the second order accurate Strömer scheme provides a stable time-discretization [19]. Here we use the same scheme to discretize (3.1),

$$\rho\frac{\mathbf{u}^{m+1}-2\mathbf{u}^m+\mathbf{u}^{m-1}}{\Delta t^2}=\mathbf{L}_h(\lambda_0,\mu_0)\mathbf{u}^m-\sum_{\nu=1}^n\mathbf{L}_h(\lambda_\nu,\mu_\nu)\bar{\mathbf{u}}^{(\nu),m}+\mathbf{F}^m, \qquad (4.1a)$$

$$\mathbf{u}^0=\mathbf{f}_0, \qquad \mathbf{u}^{-1}=\tilde{\mathbf{f}}_1, \qquad (4.1b)$$

for $m=0,1,\cdots$, where the grid index (i,j,k) has been suppressed to improve readability. There are several ways of discretizing the memory variables $\bar{\mathbf{u}}^{(\nu)}$ in time. As for the continuous and the semi-discrete cases, we choose to work with the differential equation (1.8) rather than the integral equation (1.7). If $\mathbf{u}^m$ was already known, it is not hard to verify that the discretization

$$\frac{1}{\omega_\nu}\frac{1}{2\Delta t}\big(\bar{\mathbf{u}}^{(\nu),m+1}-\bar{\mathbf{u}}^{(\nu),m-1}\big)+\frac{1}{2}\big(\bar{\mathbf{u}}^{(\nu),m+1}+\bar{\mathbf{u}}^{(\nu),m-1}\big)=\mathbf{u}^m, \qquad \nu=1,2,\cdots,n \qquad (4.2)$$

would be unconditionally stable. The subject of this section is to investigate the stability of the coupled system (4.1)-(4.2).

The following lemma gives the discrete statement of decreasing energy, corresponding to (2.11).

Lemma 4.1. *The solution of* (4.1), (4.2) *with* $\mathbf{F}^m=0$ *satisfies the discrete energy estimate*

$$e^{m+\frac{1}{2}}=e^{m-\frac{1}{2}}+B_0^{(h)}\big(\mathbf{u}^{m+1}-\mathbf{u}^{m-1},\mathbf{u}^m\big)-\sum_{\nu=1}^n B_\nu^{(h)}\big(\mathbf{u}^{m+1}-\mathbf{u}^{m-1},\bar{\mathbf{u}}^{(\nu),m}\big)$$

$$-\frac{1}{2\Delta t}\sum_{\nu=1}^n\frac{1}{\omega_\nu}S_\nu^{(h)}\big(\bar{\mathbf{u}}^{(\nu),m+1}-\bar{\mathbf{u}}^{(\nu),m-1},\bar{\mathbf{u}}^{(\nu),m+1}-\bar{\mathbf{u}}^{(\nu),m-1}\big), \qquad (4.3)$$

where the discrete energy is defined by

$$
e^{m+\frac{1}{2}} = \left\| \sqrt{\rho} \frac{\mathbf{u}^{m+1} - \mathbf{u}^m}{\Delta t} \right\|_h^2 + \frac{1}{4} S_0^{(h)} \left(\mathbf{u}^{m+1} + \mathbf{u}^m, \mathbf{u}^{m+1} + \mathbf{u}^m \right)
$$

$$
- \frac{1}{4} S_0^{(h)} \left(\mathbf{u}^{m+1} - \mathbf{u}^m, \mathbf{u}^{m+1} - \mathbf{u}^m \right) - \frac{1}{4} \sum_{\nu=1}^n S_\nu^{(h)} \left(\mathbf{u}^{m+1} + \mathbf{u}^m, \mathbf{u}^{m+1} + \mathbf{u}^m \right)
$$

$$
- \frac{1}{4} \sum_{\nu=1}^n S_\nu^{(h)} \left(\mathbf{u}^{m+1} - \mathbf{u}^m, \mathbf{u}^{m+1} - \mathbf{u}^m \right) + P^{m+\frac{1}{2}} \tag{4.4}
$$

and the term $P^{m+1/2}$ is given by

$$
P^{m+\frac{1}{2}} = \frac{1}{2} \sum_{\nu=1}^n S_\nu^{(h)} \left(\mathbf{u}^{m+1} - \bar{\mathbf{u}}^{(\nu),m}, \mathbf{u}^{m+1} - \bar{\mathbf{u}}^{(\nu),m} \right) + \frac{1}{2} \sum_{\nu=1}^n S_\nu^{(h)} \left(\mathbf{u}^m - \bar{\mathbf{u}}^{(\nu),m+1}, \mathbf{u}^m - \bar{\mathbf{u}}^{(\nu),m+1} \right).
$$

Proof. See Appendix C.   □

We can now state our main result for the fully discrete problem.

Theorem 4.1. *Assume that*

$$
\mu_0 - \sum_{\nu=1}^n \mu_\nu \geq \tilde{\mu}_{\min} > 0, \qquad \lambda_0 - \sum_{\nu=1}^n \lambda_\nu \geq \tilde{\lambda}_{\min} > 0, \tag{4.5a}
$$

$$
\rho \geq \rho_{\min} > 0, \quad \mu_\nu \geq \mu_{\min} > 0, \quad \lambda_\nu \geq \lambda_{\min} > 0, \quad \nu = 1, 2, \cdots, n, \tag{4.5b}
$$

at all grid points, and that the time-step satisfies the CFL-restriction

$$
\Delta t \leq \Delta t_{\max} = \frac{2\sqrt{1-\alpha}}{\sqrt{\zeta_{\max}}}, \qquad \zeta_{\max} = \max_{\mathbf{v} \neq \mathbf{0}} \frac{\sum_{\nu=0}^n S_\nu^{(h)}(\mathbf{v},\mathbf{v})}{(\mathbf{v},\rho\mathbf{v})_h}, \tag{4.6}
$$

where $0 < \alpha \ll 1$ is a positive constant. Then, the solution of (4.1)-(4.2) with $\mathbf{F}^m = 0$ subject to either the boundary condition (3.6), or (3.7), satisfies the energy estimate

$$
\alpha \left\| \sqrt{\rho} \frac{\mathbf{u}^{m+1} - \mathbf{u}^m}{\Delta t} \right\|_h^2 \leq e^{m+\frac{1}{2}} \leq e^{m-\frac{1}{2}} \leq \cdots \leq e^{\frac{1}{2}}, \qquad \text{any } m \geq 1.
$$

Proof. Each one of the boundary conditions (3.6)-(3.7) make the boundary terms $B_0^{(h)} - \sum_{\nu=1}^n B_\nu^{(h)}$ vanish in identity (4.3). Furthermore, the right hand side of (4.3) is non-positive because $S_\nu^{(h)}(\mathbf{v},\mathbf{v})$ is non-negative. Therefore,

$$
e^{m+\frac{1}{2}} \leq e^{m-\frac{1}{2}}.
$$

To show the lower bound on the discrete energy (defined by (4.4)), we first observe that $S_\nu^{(h)}$ depends linearly on the material coefficients λ_ν and μ_ν. Recall the definitions of

$\tilde{\lambda}$ and $\tilde{\mu}$ from (2.16). We note that

$$\frac{1}{4}S_0^{(h)}\big(\mathbf{u}^{m+1}+\mathbf{u}^m,\mathbf{u}^{m+1}+\mathbf{u}^m\big)-\frac{1}{4}\sum_{\nu=1}^n S_\nu^{(h)}\big(\mathbf{u}^{m+1}+\mathbf{u}^m,\mathbf{u}^{m+1}+\mathbf{u}^m\big)$$
$$=\frac{1}{4}\tilde{S}^{(h)}\big(\mathbf{u}^{m+1}+\mathbf{u}^m,\mathbf{u}^{m+1}+\mathbf{u}^m\big),$$

where $\tilde{S}^{(h)}(\mathbf{u},\mathbf{u})$ is defined in the same way as $S_0^{(h)}(\mathbf{u},\mathbf{u})$, but with $\tilde{\lambda}$ and $\tilde{\mu}$ replacing λ_0 and μ_0, respectively. Because of (4.5a), $\tilde{\lambda}>0$ and $\tilde{\mu}>0$, so

$$\tilde{S}^{(h)}\big(\mathbf{u}^{m+1}+\mathbf{u}^m,\mathbf{u}^{m+1}+\mathbf{u}^m\big)\geq 0 \qquad (4.7)$$

for all $\mathbf{u}^{m+1}+\mathbf{u}^m$. Secondly, the terms in (4.4) that depend on $\mathbf{v}=\mathbf{u}^{m+1}-\mathbf{u}^m$ can be bounded from below because of the inequality

$$(\mathbf{v},\rho\mathbf{v})_h-\frac{\Delta t^2}{4}\sum_{\nu=0}^n S_\nu^{(h)}(\mathbf{v},\mathbf{v})\geq\alpha(\mathbf{v},\rho\mathbf{v})_h=\alpha\|\sqrt{\rho}\mathbf{v}\|_h^2, \qquad \alpha>0. \qquad (4.8)$$

To show (4.8), first note that it holds for $\mathbf{v}=0$. Assuming that $\mathbf{v}\neq 0$, we obtain

$$\frac{\Delta t^2}{4}\frac{\sum_{\nu=0}^n S_\nu^{(h)}(\mathbf{v},\mathbf{v})}{(\mathbf{v},\rho\mathbf{v})_h}\leq 1-\alpha \qquad (4.9)$$

by a simple rearrangement of (4.8). The time step restriction (4.6) shows that (4.8) holds. Finally, because of (4.7), (4.8), and $P^{m+1/2}\geq 0$, the lower bound

$$\alpha\left\|\sqrt{\rho}\frac{\mathbf{u}^{m+1}-\mathbf{u}^m}{\Delta t}\right\|_h^2\leq e^{m+\frac{1}{2}}$$

follows from (4.4).   □

Theorem 4.1 shows that the discretization (4.1), (4.2) is stable in the energy semi-norm and, furthermore, that the forward in time difference $(\mathbf{u}^{m+1}-\mathbf{u}^m)/\Delta t$ is bounded. The upper bound depends on the initial energy, $e^{1/2}$, which obviously can be bounded independent of the grid size h if the initial data is bounded and sufficiently smooth. More precise estimates would be obtained if the spatial terms in the energy,

$$\frac{1}{4}S_0^{(h)}\big(\mathbf{u}^{m+1}+\mathbf{u}^m,\mathbf{u}^{m+1}+\mathbf{u}^m\big)-\frac{1}{4}\sum_{\nu=1}^n S_\nu^{(h)}\big(\mathbf{u}^{m+1}+\mathbf{u}^m,\mathbf{u}^{m+1}+\mathbf{u}^m\big)$$

could be bounded from below by $c\|\mathbf{u}^{m+1}+\mathbf{u}^m\|_h^2$, with c being independent of h. Another way of stating this property is that the smallest eigenvalue of the spatial operator can be bounded away from zero, independently of h. While it is relatively straight forward to obtain a lower bound of the spatial operator in terms of the symmetric part of

the discrete solution gradient (similar to (2.10) in the continuous case), it is not possible to include all terms of the discrete gradient, or $\|\mathbf{u}\|_h$, in the bound. The reason is that $S^{(h)}(\mathbf{u},\mathbf{u})$ has a six-dimensional null-space (see Appendix B), so $S^{(h)}=0$ for some non-trivial functions. Such a bound can only be obtained if additional conditions are imposed that remove all rigid body components from the solution. One way of obtaining such a bound is to impose a Dirichlet boundary condition on at least one side of the computational domain. We assert that a discrete version of Korn's inequality [11] holds in this case, but we only have an outline of a rather technical and lengthy proof. However, similar results have been proven for finite difference approximations of the two-dimensional elastostatic equations, with a free surface boundary condition on one side of the computational domain and Dirichlet conditions on the other three sides, see [9].

The spectral radius $\zeta_{\max}$, which is needed to determine the time step, can be difficult to calculate, especially when the material properties are heterogeneous and unsmooth. For simulations of the purely elastic wave equation, we have developed the following technique. We first use a von Neumann analysis to evaluate the largest stable local time step at each grid point. This estimate uses the local material properties in a homogeneous material model, assumes periodic boundary conditions to allow an explicit evaluation of the largest stable local time step. The estimated time step is then taken as the minimum of all local time steps. The presence of free surface boundary conditions can impose further restrictions on the time step [19]. Unsmooth material properties can also require the time step to be reduced. Both these effects are accounted for by using a time step which is about 15 percent smaller than the estimated value.

Based on the observation that the sum $\sum_{\nu=0}^n S_\nu^{(h)}(\mathbf{v},\mathbf{v})$ is linear in the material data, the spectral radius for the viscoelastic wave equation can be estimated in the same way as for the purely elastic wave equation, simply by replacing μ_0 and λ_0 by the sums $\sum_{\nu=0}^n \mu_\nu$ and $\sum_{\nu=0}^n \lambda_\nu$, respectively. Since $\lambda_\nu > 0$ and $\mu_\nu > 0$ for all $\nu = 0,1,\cdots,n$, the time step must always be reduced when viscoelastic terms are included. However, because of material condition (4.5a),

$$\sum_{\nu=0}^n \mu_\nu < 2\mu_0 \quad \text{and} \quad \sum_{\nu=0}^n \lambda_\nu < 2\lambda_0.$$

Consequently, the spectral radius of the spatial operator for the viscoelastic problem is at most a factor of two larger than in the corresponding elastic case, and the time step never needs to be reduced by more than a factor of $\sqrt{2}$.

5   Determining model parameters

To make the presentation self-contained, we need to state some well-known results from the theory of viscoelastic materials. We suggest the book by Carcione [4] for a more thorough presentation of this theory.

In frequency space, the viscoelastic shear modulus is defined in terms of the Fourier

transform of the stress relaxation function (1.2),

$$\hat{M}_S(\omega) =: i\omega\hat{\mu}(\omega) = \mu_0 - \sum_{\nu=1}^{n} \frac{\mu_\nu}{1+i\omega/\omega_\nu}, \tag{5.1}$$

where ω is the dual variable of t, and μ_0 is called the unrelaxed shear modulus.

The quality factor for shear waves is defined by

$$Q_S(\omega) =: \frac{\text{Re } \hat{M}_S(\omega)}{\text{Im } \hat{M}_S(\omega)} = \frac{1 - \sum_{\nu=1}^{n} \dfrac{\beta_\nu \omega_\nu^2}{\omega_\nu^2 + \omega^2}}{\sum_{\nu=1}^{n} \dfrac{\beta_\nu \omega\omega_\nu}{\omega_\nu^2 + \omega^2}}, \qquad \beta_\nu = \frac{\mu_\nu}{\mu_0}. \tag{5.2}$$

To obtain a linear least squares problem for the β_ν coefficients, we follow the approach laid out by Emmerich and Korn [8]. Relation (5.2) is re-written as

$$\frac{1}{Q_S(\omega)} = \sum_{\nu=1}^{n} \frac{\beta_\nu \omega\omega_\nu}{\omega_\nu^2 + \omega^2} + \frac{1}{Q_S(\omega)} \sum_{\nu=1}^{n} \frac{\beta_\nu \omega_\nu^2}{\omega_\nu^2 + \omega^2} = \sum_{\nu=1}^{n} \beta_\nu \frac{\omega\omega_\nu + \omega_\nu^2/Q_S(\omega)}{\omega_\nu^2 + \omega^2}. \tag{5.3}$$

The relaxation frequencies, ω_ν, are evenly distributed in a logarithmic sense over the frequency band $[\omega_{\min}, \omega_{\max}]$, i.e.,

$$\omega_\nu = \omega_{\min} r^{(\nu-1)}, \quad \nu = 1, 2, \cdots, n, \quad r = \left(\frac{\omega_{\max}}{\omega_{\min}}\right)^{\frac{1}{(n-1)}}.$$

Setting $Q_S(\omega_k^{(c)}) = Q_0 = \text{const.}$ in (5.3) at $2n-1$ collocation frequencies $\omega_k^{(c)}$, which also are distributed logarithmically over the same frequency band, results in $2n-1$ linear equations for the n coefficients β_ν. This over-determined linear system is solved in the least squares sense.

To choose the unrelaxed shear modulus μ_0, we need to study the wave propagation speed in a viscoelastic material. Consider the one-dimensional half-line problem

$$\rho u_{tt} = \sigma_x, \qquad x \geq 0, \quad t \geq 0, \tag{5.4a}$$
$$u(0,t) = g(t), \qquad t \geq 0, \tag{5.4b}$$

where $\sigma(x,t)$ is the viscoelastic stress. In one space dimension, the strain is given by $\epsilon = u_x$, and the stress satisfies

$$\sigma(t) = \int_{-\infty}^{t} \mu(t-\tau) \frac{\partial \epsilon}{\partial t}(\tau) d\tau. \tag{5.5}$$

After Fourier transforming (5.5), we get

$$\hat{\sigma}(\omega) = \hat{\mu}(\omega) i\omega\hat{\epsilon}(\omega) =: \hat{M}_S(\omega)\hat{\epsilon}(\omega). \tag{5.6}$$

Fourier transforming (5.4a), (5.4b) and using (5.6), gives

$$\rho\omega^2\hat{u}+\hat{M}_S\hat{u}_{xx}=0, \qquad x\geq 0, \quad -\infty<\omega<\infty,$$
$$\hat{u}(0,\omega)=\hat{g}(\omega), \qquad -\infty<\omega<\infty,$$

which is solved by

$$\hat{u}(x,\omega)=\hat{g}(\omega)e^{i\omega x\sqrt{\rho/\hat{M}_S}}, \qquad \mathrm{Re}\left(i\omega\sqrt{\rho/\hat{M}_S}\right)<0.$$

The loss angle, δ, is defined by $\tan\delta=1/Q_S$. By writing $\hat{M}_S=|\hat{M}_S|(\cos(\delta)+i\sin(\delta))$, the appropriate root is given by

$$\sqrt{\frac{\rho}{\hat{M}_S}}=-\rho^{\frac{1}{2}}|\hat{M}_S|^{-\frac{1}{2}}\left(\cos\left(\frac{\delta}{2}\right)-i\sin\left(\frac{\delta}{2}\right)\right).$$

For harmonic boundary data, $g(t)=e^{i\omega t}$, the solution can be written

$$u(x,t)=e^{i\omega(t-x/c_s)}e^{-\alpha|\omega|x}, \qquad c_s=\frac{|\hat{M}_S|^{\frac{1}{2}}}{\rho^{\frac{1}{2}}\cos(\delta/2)}, \qquad \alpha=\frac{1}{c_s}\tan\left(\frac{\delta}{2}\right). \qquad (5.7)$$

The wave travels to the right (increasing x) with phase velocity c_s and wave length $2\pi c_s/|\omega|$. The amplitude of the wave decays by a factor $\exp(-2\pi\tan(\delta/2))$ per wave length.

Since the phase velocity depends on ω, it is necessary to specify at what reference frequency $c_s(\omega)$ is given. The definition of the viscoelastic shear modulus (5.1) gives

$$c_s^2(\omega)=\frac{\mu_0|m_s(\omega)|}{\rho\cos^2(\delta/2)}, \qquad m_s(\omega)=1-\sum_{\nu=1}^{n}\beta_\nu\frac{\omega_\nu^2-i\omega\omega_\nu}{\omega_\nu^2+\omega^2}. \qquad (5.8)$$

The function $m_s(\omega)$ can be evaluated once β_ν and ω_ν have been determined. The unrelaxed modulus corresponding to shear speed c_s, measured at reference frequency ω_r, is then given by

$$\mu_0=\frac{\rho c_s^2(\omega_r)\cos^2(\delta/2)}{|m_s(\omega_r)|}. \qquad (5.9)$$

Once μ_0 and β_ν are determined, (5.2) gives

$$\mu_\nu=\mu_0\beta_\nu, \qquad \nu=1,2,\cdots,n.$$

Since compressional and shear waves are observed to attenuate at different rates, it is desirable to use two quality factors in the material model: Q_P and Q_S. The attenuation of compressional waves is modeled by introducing the stress-relaxation function (*not* the bulk modulus) $\kappa(t)=:\lambda(t)+2\mu(t)$, where

$$\kappa(t)=\kappa_0-\sum_{\nu=1}^{n}\kappa_\nu(1-e^{-\omega_\nu t}), \qquad \gamma_\nu=\frac{\kappa_\nu}{\kappa_0}. \qquad (5.10)$$

Corresponding to (5.1), the Fourier transform of the viscoelastic modulus for compressional waves is defined by

$$\hat{M}_P(\omega) =: i\omega\hat{\kappa}(\omega) = \kappa_0 - \sum_{\nu=1}^{n} \frac{\kappa_\nu}{1 + i\omega/\omega_\nu}.$$

The quality factor for compressional waves, Q_P, follows by replacing β_ν by γ_ν in (5.2). We substitute β_ν by γ_ν and Q_S by Q_P in (5.3) and solve for γ_ν, using the same relaxation and collocation frequencies as before.

The unrelaxed compressional modulus, κ_0, is determined by the compressional wave speed c_p, measured at reference frequency ω_r,

$$\kappa_0 = \frac{\rho c_p^2(\omega_r)\cos^2(\delta_p)}{|m_p(\omega_r)|}, \qquad m_p(\omega) = 1 - \sum_{\nu=1}^{n} \gamma_\nu \frac{\omega_\nu^2 - i\omega\omega_\nu}{\omega_\nu^2 + \omega^2},$$

where $\tan(\delta_p) = 1/Q_P$. Given κ_0 and γ_ν, we have $\kappa_\nu = \kappa_0\gamma_\nu$.

After the coefficients μ_ν and κ_ν have been determined, the coefficients of the first Lamé parameter are given by

$$\lambda_\nu = \kappa_\nu - 2\mu_\nu, \qquad \nu = 0, 1, \cdots, n. \tag{5.11}$$

5.1 Numerical evaluation of viscoelastic properties

A wave with frequency f traveling through a media with shear speed c_s has wave length $l_s = c_s/f$. On a computational grid with grid size h, the accuracy of the numerical solution can be characterized by the number of grid points per shortest wave length,

$$P_{pw} = \frac{l_s}{h} = \frac{c_s}{fh} = \frac{2\pi c_s}{\omega h}, \tag{5.12}$$

where $\omega = 2\pi f$ is the angular frequency. Depending on the order of accuracy and other details of the numerical method, the numerical solution has acceptable accuracy if the shortest wave satisfies $P_{pw} \geq P_{\min}$. For example, our second order accurate finite difference method requires $P_{\min} \approx 15$, see [21].

When modeling viscoelastic wave propagation, it is natural to let (5.12) guide the upper limit of the frequency band for approximating $Q(\omega)$,

$$\omega_{\max} = C\frac{2\pi c_s}{P_{\min}h}, \qquad C = \mathcal{O}(1). \tag{5.13}$$

The lower limit of the frequency band, $\omega_{\min}$, can be estimated using the size of the computational domain, $L_{\max}$, which in large scale three-dimensional computations often corresponds to $\mathcal{O}(100)$ of the shortest wave lengths, or more. The lowest resolvable angular frequency can therefore be estimated by

$$\omega_{\min} = \frac{2\pi c_s}{L_{\max}} \approx \frac{2\pi c_s}{100 l_s} = \frac{\omega_{\max}}{100}.$$
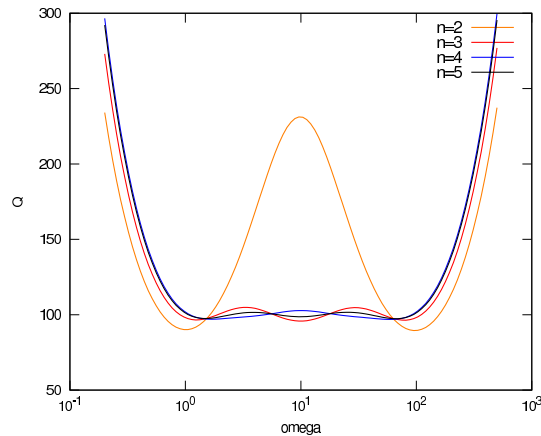
Figure 1: Actual quality factor $Q(\omega)$ approximating $Q_0 = 100$ in the frequency band $\tilde{\omega} \in [1, 100]$, for different numbers of viscoelastic mechanisms.

Hence, it is desirable for the viscoelastic model to satisfy $Q(\omega) \approx Q_0$ over two decades in frequency. As computers grow larger, it will be possible to resolve a wider range of wave lengths in numerical simulations. This will result in additional requirements on the fidelity in the viscoelastic modeling.

Because the computational cost of viscoelastic modeling increases with the number of mechanisms, n, it is desirable to use the smallest value of n that gives acceptable accuracy in the approximation of $Q(\omega)$. When evaluating the properties of the viscoelastic modulus (5.1), we note that it depends on the frequency ratios ω / ω_v. Hence, the properties of $\hat{M}$ and Q can be studied in terms of the normalized frequency

$$\tilde{\omega} = \frac{\omega}{\omega_{\min}},$$

as long as the relaxation and collocation frequencies are normalized in the same way.

We start the numerical evaluation of our viscoelastic model by evaluating the quality factor (5.2) for different number of mechanisms, n. In Fig. 1, we present $Q(\omega)$ when the coefficients β_v are chosen to approximate $Q_0 = 100$ using the above least squares procedure, in the frequency band $\tilde{\omega} \in [1, 100]$. Clearly, $n = 2$ provides inadequate modeling of a constant Q over two decades in frequency, but $n = 3$ gives a much better approximation. Increasing n further only leads to small improvements.

It is interesting to note that in all models, $Q(\omega)$ grows rapidly for $\omega > \omega_{\max}$. Hence the viscoelastic model does *not* provide significant damping of higher (poorly resolved) frequencies in the numerical solution, and does *not* act as an artificial dissipation.

To evaluate how wide the frequency band can be for different numbers of viscoelastic mechanisms, we set $\tilde{\omega}_{\min} = 1$ and study the maximum relative error,

$$e(\tilde{\omega}_{\max}) = \max_{\tilde{\omega} \in [1, \tilde{\omega}_{\max}]} \frac{|Q(\tilde{\omega}) - Q_0|}{Q_0}$$
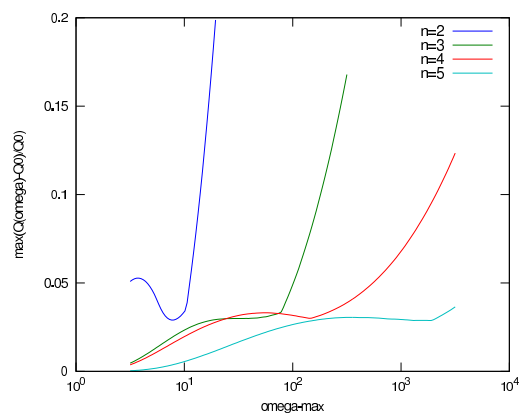
Figure 2: Max relative error $(Q(\tilde{\omega})-Q_0)/Q_0$ over the frequency band $\tilde{\omega} \in [1, \tilde{\omega}_{\max}]$, as function of $\tilde{\omega}_{\max}$. Here, $Q_0 = 100$ and the different lines correspond to different numbers of viscoelastic mechanisms.
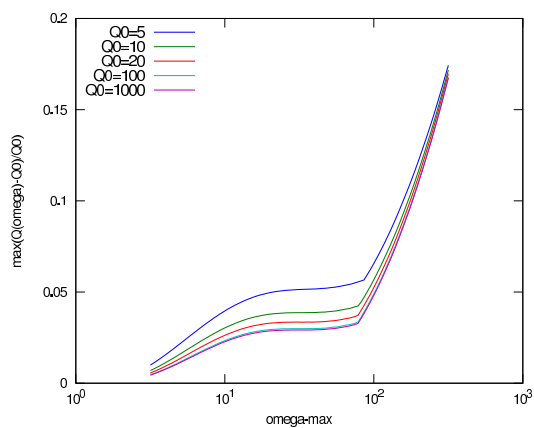

Figure 3: Max relative error $(Q(\tilde{\omega})-Q_0)/Q_0$ over the frequency band $\tilde{\omega} \in [1, \tilde{\omega}_{\max}]$, as function of $\tilde{\omega}_{\max}$. Here, the number of viscoelastic mechanisms is $n = 3$ and the different lines correspond to different values of Q_0.
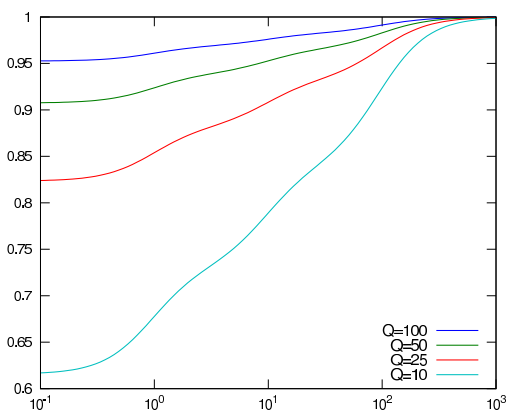

Figure 4: Relative phase velocity $|m_s|^{1/2}/\cos(\delta/2)$ over the frequency band $\tilde{\omega} \in [1, 100]$. Here, $n = 3$, and the different colors correspond to different values of Q.

as function of $\tilde{\omega}_{\max}$. In Fig. 2, we see that all values of n give small errors for sufficiently small values of $\tilde{\omega}_{\max}$, and that the error grows rapidly when the frequency band exceeds a certain width. Max relative errors of about 3% are obtained at $\tilde{\omega}_{\max} \approx 10$ for $n = 2$, at $\tilde{\omega}_{\max} \approx 80$ for $n = 3$, at $\tilde{\omega}_{\max} \approx 150$ for $n = 4$, and at $\tilde{\omega}_{\max} \approx 2000$ for $n = 5$. These findings are comparable to the results in [23].

So far, we have only evaluated the viscoelastic model for $Q_0 = 100$. To investigate how the error depends on Q_0, we take $n = 3$ and repeat the previous experiment for different values of Q_0, see Fig. 3. The results show that the error depends very weakly on Q_0 for $Q_0 \geq 100$. For smaller values of Q_0, the relative error gets larger, but the shape of the curves remains essentially unchanged. However, the relative error grows much slower than $1/Q_0$, so the absolute error gets smaller with Q_0. Also note that the value of $\tilde{\omega}_{\max} \approx 80$, beyond which the error starts to grow rapidly, is independent of Q_0.

To demonstrate how the phase velocity varies with ω, we evaluate the factor $|m^{1/2}|/\cos(\delta/2)$ in (5.8). The results shown in Fig. 4 illustrate that the frequency dependence on the phase velocity increases dramatically when Q gets smaller. Also note that the phase velocity grows approximately linearly on a logarithmic scale in ω, throughout the frequency band $[\omega_{\min}, \omega_{\max}]$. Outside this band, the phase velocity tends to constant values.

6 Numerical experiments

6.1 Comments on the implementation

Our implementation of the purely elastic wave equation [19, 20, 22], is based on the discrete formulation (4.1), with $n = 0$. This approach requires one subroutine to be implemented for evaluating the term $\mathbf{L}_h(\lambda, \mu)\mathbf{u}^m$. Note that the same subroutine can be used to evaluate the viscoelastic terms $\mathbf{L}_h(\lambda_\nu, \mu_\nu)\bar{\mathbf{u}}^{(\nu),m}$ when $n > 0$, by passing different material properties and applying it to $\bar{\mathbf{u}}^{(\nu),m}$ instead of $\mathbf{u}^m$. Hence, once the purely elastic implementation has been verified, it is rather straight forward to include viscoelastic effects in our formulation.

The memory variables do not need boundary conditions because they satisfy ordinary differential equations. That is, once $\mathbf{u}^m$ has been calculated at all grid points (including ghost points), (4.2) can be used to evaluate $\mathbf{u}^{(\nu),m+1}$ everywhere. To impose the free surface boundary condition (3.7) on $\mathbf{u}^{m+1}$, we first calculate $\mathbf{u}^{(\nu),m+1}$, which enters the free surface boundary condition as a forcing term.

The energy conserving grid refinement interface condition, described in [22], is also easily generalized to the viscoelastic case. Here, we only need to add contributions from the memory variables to the normal stresses in the grid interface equations. Compared to the grid interface coupling equations in the purely elastic case, only the right hand side in the linear system is modified. There is not enough space to present the details here, but because the boundary terms cancel along the grid refinement interface, the energy conservation at the grid interface for the purely elastic case generalizes to a proof

of energy decay for the viscoelastic equations with grid refinement interface. Some of the computations presented below use grid refinements, and illustrate the accuracy and computational efficiency of this approach.

All calculations in this section were obtained with version 2.1 of the parallel open source code WPP [21].

6.2 Method of manufactured solutions

We start by evaluating the error in the numerical solution, when both the material and the solution are smooth. Let the computational domain be the cube $(x,y,z) \in [0,5]^3$, impose a free surface boundary condition on the $z = 0$ boundary and Dirichlet conditions on all other boundaries. The test will use one viscoelastic mechanism ($n = 1$). We take the material properties to be

$$\rho(x,y,z) = A_\rho \big(2 + \sin(\omega_m x + \theta_m) \cos(\omega_m y + \theta_m) \sin(\omega_m z + \theta_m) \big),$$

$$\mu_0(x,y,z) = A_\mu \big(3 + \cos(\omega_m x + \theta_m) \sin(\omega_m y + \theta_m) \sin(\omega_m z + \theta_m) \big),$$

$$\lambda_0(x,y,z) = A_\lambda \big(2 + \sin(\omega_m x + \theta_m) \sin(\omega_m y + \theta_m) \cos(\omega_m z + \theta_m) \big),$$

$$\mu_1(x,y,z) = A_\mu \left(\frac{3}{2} + \frac{1}{2} \cos(\omega_m x + \theta_m) \cos(\omega_m y + \theta_m) \sin(\omega_m z + \theta_m) \right),$$

$$\lambda_1(x,y,z) = A_\lambda \left(\frac{1}{2} + \frac{1}{4} \sin(\omega_m x + \theta_m) \cos(\omega_m y + \theta_m) \sin(\omega_m z + \theta_m) \right),$$

where $\omega_m = 3.2$, $\theta_m = 0.8$, $A_\rho = 2$, $A_\mu = 3$, and $A_\lambda = 1$. Note that these material parameters satisfy conditions (4.5a)-(4.5b) of Theorem 4.1. The internal forcing, boundary forcing and initial conditions are chosen such that the exact (manufactured) solution becomes

$$u_e(x,y,z,t) = \sin(\omega(x - c_e t)) \sin(\omega y + \theta) \sin(\omega z + \theta), \tag{6.1a}$$

$$v_e(x,y,z,t) = \sin(\omega x + \theta) \sin(\omega(y - c_e t)) \sin(\omega z + \theta), \tag{6.1b}$$

$$w_e(x,y,z,t) = \sin(\omega x + \theta) \sin(\omega y + \theta) \sin(\omega(z - c_e t)), \tag{6.1c}$$

$$\overline{u}_e(x,y,z,t) = \cos(\omega(x - c_e t) + \theta) \sin(\omega x + \theta) \cos(\omega(z - c_e t) + \theta), \tag{6.1d}$$

$$\overline{v}_e(x,y,z,t) = \sin(\omega(x - c_e t)) \cos(\omega(y - c_e t) + \theta) \cos(\omega z + \theta), \tag{6.1e}$$

$$\overline{w}_e(x,y,z,t) = \cos(\omega x + \theta) \cos(\omega y + \theta) \sin(\omega(z - c_e t) + \theta), \tag{6.1f}$$

with $\omega = 3$, $\theta = 0.2$, and $c_e = 1.3$. Here, $\mathbf{\overline{u}}^{(1)} = (\overline{u}, \overline{v}, \overline{w})$. Table 1 gives the errors in the numerical solution, evaluated in maximum norm for both the displacement and the memory variables at time $t = 4.8$, for different grid sizes. The maximum norm is computed over the computational domain and over the three components of the vector variables. The errors in both variables clearly decrease as $\mathcal{O}(h^2)$.

Next, we perform the same test with the same data, but on a composite grid with one base grid and one refinements. The base grid has grid size $2h$ in $2 \le z \le 5$ and the refined grid has size h in $0 \le z \le 2$. In terms of the number of grid points in the x-direction on the

Table 1: Errors in the numerical solution at time $t = 4.8$, on a uniform grid, when the exact solution is (6.1). Here, p and $\overline{p}$ are convergence exponents for $\mathbf{u}$ and $\bar{\mathbf{u}}^{(1)}$, respectively.

N_x	h	$\|\mathbf{u}(\cdot,t) - \mathbf{u}_e(\cdot,t)\|_\infty$	$\|\bar{\mathbf{u}}^{(1)}(\cdot,t) - \bar{\mathbf{u}}_e^{(1)}(\cdot,t)\|_\infty$	p	$\overline{p}$
31	1.67×10^{-1}	1.63×10^{-1}	1.19×10^{-1}	–	–
61	8.33×10^{-2}	4.74×10^{-2}	3.45×10^{-2}	1.78	1.79
121	4.17×10^{-2}	1.24×10^{-2}	9.14×10^{-3}	1.93	1.92
241	2.08×10^{-2}	3.15×10^{-3}	2.33×10^{-3}	1.98	1.97

Table 2: Errors in the numerical solution at time $t = 4.8$, on a composite grid, when the exact solution is (6.1). Here, p and $\overline{p}$ are convergence exponents for $\mathbf{u}$ and $\bar{\mathbf{u}}^{(1)}$, respectively.

N_x	$2h$	$\|\mathbf{u}(\cdot,t) - \mathbf{u}_e(\cdot,t)\|_\infty$	$\|\bar{\mathbf{u}}^{(1)}(\cdot,t) - \bar{\mathbf{u}}_e^{(1)}(\cdot,t)\|_\infty$	p	$\overline{p}$
31	1.67×10^{-1}	1.18×10^{-1}	9.73×10^{-2}	–	–
61	8.33×10^{-2}	2.90×10^{-2}	2.41×10^{-2}	2.02	2.01
121	4.17×10^{-2}	7.36×10^{-3}	5.97×10^{-3}	1.99	2.01

base grid, the grid sizes are

$$2h = \frac{5}{N_x - 1}, \qquad h = \frac{5}{2(N_x - 1)},$$

in the base and refined grids, respectively. Table 2 gives the errors in the numerical solutions, evaluated in maximum norm for both the displacements and the memory variables at time $t = 4.8$. Table 2 shows that both errors are of the order $\mathcal{O}(h^2)$.

This test verifies that the implementation is second order accurate, and also supports our mathematical results concerning the stability of the method.

6.3   Point source in a uniform material

To evaluate the convergence properties of our scheme and the influence of the number of viscoelastic mechanisms, we consider the half-space problem with homogeneous material properties (using SI units): $\rho = 2{,}650$, $c_s = 2{,}000$, $c_p = 4{,}000$, $Q_P = 200$, and $Q_S = 100$. In the simulation, the half-space $z \geq 0$ is truncated to the computational domain $(x,y) \in [0, 4 \times 10^4]^2$, $z \in [0, 2 \times 10^4]$. A small earthquake is modeled by placing a moment tensor point source at location $\mathbf{x}_s$, using the forcing function

$$\mathbf{F}(\mathbf{x},t) = g(t)\mathcal{M}\nabla\delta(\mathbf{x} - \mathbf{x}_s), \qquad \mathcal{M} = 10^{18} \begin{pmatrix} 0 & 1 & 0 \\ 1 & 0 & 0 \\ 0 & 0 & 0 \end{pmatrix} \tag{6.2}$$

located at $\mathbf{x}_s = 10^4 (2, 2, 0.21)^T$. Here $\nabla\delta$ denotes the gradient of the Dirac distribution. We use the second order accurate technique described in [22] to discretize the singular source
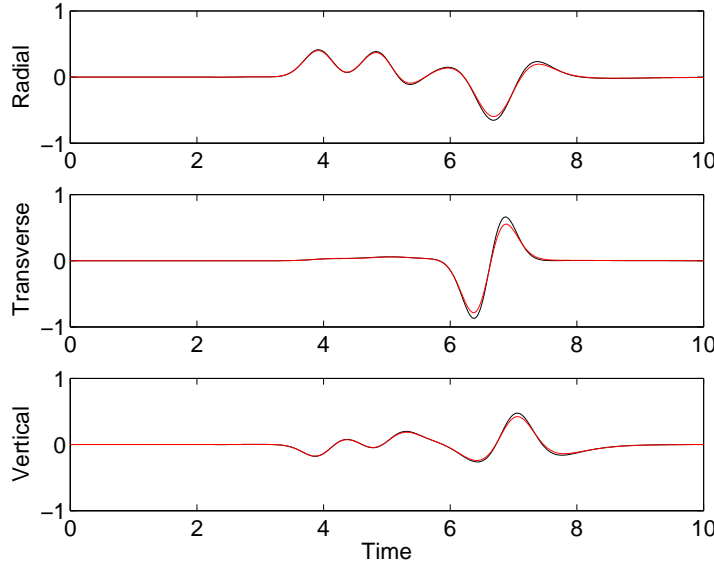
Figure 5: Semi-analytical solutions as function of time at receiver location $x_r = 2.6 \times 10^4$, $y_r = 2.8 \times 10^4$, $z_r = 0$ in a homogeneous material. The red line corresponds to the solution in a viscoelastic material with $Q_P = 200$ and $Q_S = 100$. The black line corresponds to a purely elastic material with the same density and wave speeds as in the viscoelastic material.

term. The time-function is given by the Gaussian,

$$g(t) = \frac{1}{\sigma\sqrt{2\pi}} e^{-\frac{(t-t_0)^2}{2\sigma^2}} \tag{6.3}$$

with spread $\sigma = 0.25$ and offset $t_0 = 1.5$. Using notation from seismology, this moment tensor point source is characterized by the seismic moment $m_0 = 10^{18}$ and the angles dip=90°, rake=0°, and strike=0° (when the x-axis is directed towards North), see [1]. The solution is recorded in time at $x_r = 2.6 \times 10^4$, $y_r = 2.8 \times 10^4$, $z_r = 0$ and compared to a semi-analytical frequency-wavenumber (FK) solution [26] using the FK code [25]. This solution is denoted $\mathbf{u}_s(\mathbf{x}_r, t)$. An example is shown in Fig. 5, where we present the radial, transverse, and vertical components of the solution, illustrating the effects of viscoelasticity. These components are defined in a polar coordinate system centered at the (x, y)-location of the source, with the vertical component in the z-direction (positive down), i.e., $u_{vert} = w$. Since $x_r - x_s = 6 \times 10^3$, $y_r - y_s = 8 \times 10^3$, the radial component is $u_{rad} = 0.6u + 0.8v$, and the transverse component is $u_{tran} = -0.8u + 0.6v$.

We measure the error in the time interval $0 \leq t \leq T$ using the L_2-norm in time, i.e.,

$$\|\mathbf{u}(\mathbf{x}_r, \cdot)\|_2^2 = \frac{1}{T} \int_0^T \left(u_{rad}(\mathbf{x}_r, t)^2 + u_{tran}(\mathbf{x}_r, t)^2 + u_{vert}(\mathbf{x}_r, t)^2 \right) dt. \tag{6.4}$$

We estimate the convergence rate using the formula $p_2(h) = \log_2(e(2h)/e(h))$, where $e(h)$ is the norm of the error in the solution with grid size h.

Table 3: Errors and convergence rates in the numerical solution when the material is homogeneous in space. The norms are taken over the period $0 \leq t \leq 10$.

	Uniform grid			Composite grid	
h	$\|\mathbf{u}(\mathbf{x}_r,\cdot) - \mathbf{u}_s(\mathbf{x}_r,\cdot)\|_2$	p_2	h	$\|\mathbf{u}(\mathbf{x}_r,\cdot) - \mathbf{u}_s(\mathbf{x}_r,\cdot)\|_2$	p_2
200	1.08×10^{-1}	–	400/200	2.32×10^{-1}	–
100	2.82×10^{-2}	1.94	200/100	6.96×10^{-2}	1.73
50	7.40×10^{-3}	1.93	100/50	1.59×10^{-2}	2.12

A free surface boundary condition is imposed on the $z = 0$ boundary and homogeneous Dirichlet conditions are used on all other boundaries together with a damping sponge layer, which reduces artificial reflections. Three viscoelastic mechanism were used in these experiments with $\omega_1/2\pi = 0.05$, $\omega_2/2\pi = 0.5$ and $\omega_3/2\pi = 5$. The phase velocities were specified at reference frequency 1Hz.

We first discretize the computational domain on a uniform grid and study the error for the grid sizes $h = 400$, 200, and 100, see Table 3. We then repeat the experiment using a composite grid, where a fine grid with size h discretizes $0 \leq z \leq 1,000$, and a coarser grid with size $2h$ is used for $z \geq 1,000$. Our results indicate that the solutions on both grid configurations converge to zero as $\mathcal{O}(h^2)$, when the grid is sufficiently fine. Note that the error levels for each composite grid are in between those on uniform grids with the same grid sizes as in the base and refined grids, respectively.

6.4   The LOH.3 layer over half-space problem

We consider test problem LOH.3 which was used by Day et al. [5] to evaluate the accuracy of anelastic attenuation in seismic wave propagation codes. This test uses a simple material model with piecewise constant material properties. In the top layer ($0 \leq z \leq 1,000$), the material properties are (in SI units) $\rho = 2,600$, $c_p = 4,000$, $c_s = 2,000$, $Q_P = 120$, and $Q_S = 40$. In the half-space below the top layer ($z > 1,000$), the material properties are $\rho = 2,700$, $c_p = 6,000$, $c_s = 3,464$, $Q_P = 155.9$, and $Q_S = 69.3$. Phase velocities are given at reference frequency 2.5Hz. We model the half-space problem using a computational domain of size $(x,y) \in [0,40000]^2$ and $0 \leq z \leq 20000$. As before, a free surface boundary condition is imposed on the $z = 0$ boundary, and homogeneous Dirichlet conditions together with a sponge layer are used to reduce artificial reflections from all other boundaries. A small earthquake is modeled by the moment tensor point source (6.2) located at $x_s = 20,000$, $y_s = 20,000$, at depth $z_s = 2,000$. The time-function is given by the Gaussian (6.3) with spread $\sigma = 0.05$ and offset $t_0 = 0.2$, corresponding to the center frequency $f_0 \approx 3.18$Hz. We evaluate the solution at receiver # 10, located at $x_r = 26,000$, $y_r = 28,000$, $z_r = 0$. A semi-analytical frequency-wavenumber solution was obtained using a modified version of the method described in Apsel and Luco [2]. This solution is denoted $\mathbf{u}_e(\mathbf{x}_r,t)$.

The velocity structure of this problem makes it an ideal candidate for grid refinement, and we use a fine grid with size $h = 25$ in the top layer ($0 \leq z \leq 1000$) and a base grid with size $h = 50$ in the half-space $z \geq 1,000$, resulting in a computational mesh with approxi-
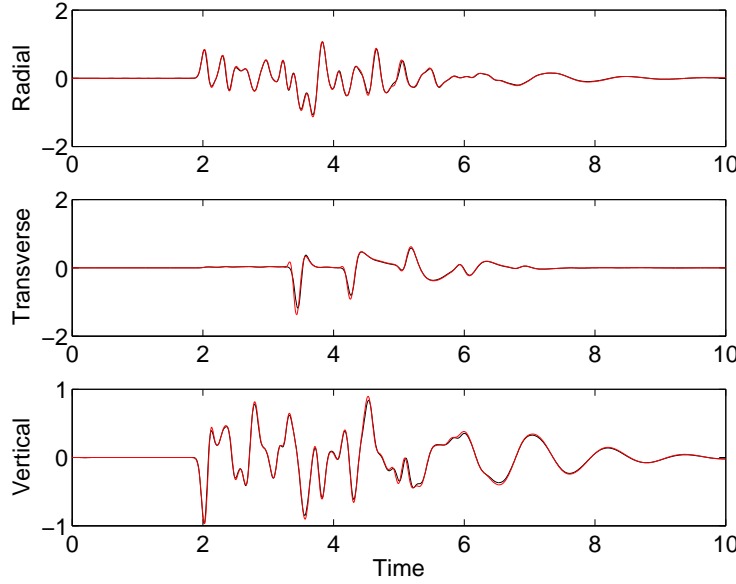
Figure 6: Solution of the LOH.3 test problem at receiver # 10. The black line is the semi-analytical solution, and the red line shows the numerical solutions with $n=3$ mechanisms.

mately 349 million grid points. At this resolution, the discretization errors are sufficiently small to distinguish the influence of the number of mechanisms, n, in the viscoelastic model. In all cases, the lowest and highest relaxation frequencies were $\omega_1/2\pi = 0.15$Hz and $\omega_n/2\pi = 15$Hz, respectively. We ran the simulations to end time $T = 10$, corresponding to approximately 2560 time steps (the exact number depends on n). The simulations were performed on 64 nodes on the Atlas Linux cluster at LLNL, where each node has 8 cores. The L_2-norm of the error in the numerical solutions, as well as the CPU time, are reported in Table 4. The error is significantly smaller with $n=3$ mechanisms than with $n=2$. However, the error does not decrease further for $n=4$, which indicates that discretization errors dominate the overall error at this grid resolution. Our results in Section 5.1 only show minor improvements of the modeling error between $n=3$ and $n=4$. A significant reduction of the grid size would probably be necessary to make the modeling error discernible for $n>3$. However, grid refinement is computationally expensive. For example, reducing the grid size by a factor of two would result in a mesh with ap-

Table 4: CPU timings and L_2 norm of the error in the numerical solution of the LOH.3 test problem, for different number of viscoelastic mechanisms.

n	$\|\mathbf{u}(\mathbf{x}_r,\cdot) - \mathbf{u}_e(\mathbf{x}_r,\cdot)\|_2$	CPU time (64 nodes $\times$ 8 cores)
2	1.31×10^{-1}	25 min., 30 sec.
3	4.84×10^{-2}	31 min., 14 sec.
4	5.09×10^{-2}	36 min., 7 sec.

proximately 2.8 billion (10^9) grid points, and twice the number of time steps would be required to advance the solution to the same end time. Unfortunately, we did not have access to sufficiently large computational resources for repeating the numerical experiment on such a fine grid.

A visual comparison of the semi-analytical and the numerical solutions with $n = 3$ mechanisms can be found in Fig. 6. We note that the agreement is very good in general, but some overshoots are distinguishable in the transverse component. To estimate the number of grid points per shortest wave length, we evaluate (5.12) using the highest significant frequency in the source time-function,

$$f_{up} \approx 2.5 \frac{1}{2\pi\sigma} = \frac{50}{2\pi}, \qquad P_{pw} = \frac{c_s}{f_{up}h} = \frac{2000 \times 2\pi}{50 \times 25} \approx 10.05.$$

7 Conclusions

We have described an energy stable finite difference approximation of the three-dimensional viscoelastic wave equation with an n-SLS material model. The proposed scheme discretizes the governing equations in second order displacement formulation using $3n$ memory variables, making it significantly more memory efficient than the commonly used first order velocity-stress formulation. The discretization is a generalization of our summation-by-parts finite difference discretization of the elastic wave equation [19, 20, 22]. We have derived sufficient conditions on the material parameters for well-posedness of the viscoelastic wave equation. We have also proven that our scheme is stable and satisfies an energy estimate under two conditions. First, the material parameters must satisfy the conditions for well-posedness and, secondly, the time step must satisfy a CFL-type time step restriction.

The new method has been implemented as part of version 2.1 of the open source software WPP [21], which also allows for grid refinements with hanging nodes as well as free surface boundaries on realistic topographies.

Plans for the near future include generalizations to fourth order accuracy. This will improve the efficiency of the method in terms of the number of grid points per wave length that is required to obtain a given accuracy. A smaller discretization error might make it necessary to also reduce the viscoelastic modeling error, which can be done by increasing the number of viscoelastic mechanisms.

Acknowledgments

A Detailed expression for $S_\nu^{(h)}(\mathbf{v},\mathbf{u})$

A detailed expression for $S_\nu^{(h)}(\mathbf{v},\mathbf{u})$ was derived in [20]. Here we re-state the result using the vector notation $\mathbf{v}=(v^1,v^2,v^3)^T$ and $\mathbf{u}=(u^1,u^2,u^3)^T$. For simplicity we drop subscript ν on $S^{(h)}$, λ, and μ. We have,

$$S^{(h)}(\mathbf{v},\mathbf{u})_h = A(\mathbf{v},\mathbf{u}) + \frac{h^2}{4}R(\mathbf{v},\mathbf{u}), \tag{A.1}$$

where

$$
\begin{aligned}
A(\mathbf{v},\mathbf{u}) =& 2(D_+^x v^1, E_{\frac{1}{2}}^x(\mu)D_+^x u^1)_{mx} + 2(D_+^y v^2, E_{\frac{1}{2}}^y(\mu)D_+^y u^2)_{my} + 2(D_+^z v^3, E_{\frac{1}{2}}^z(\mu)D_+^z u^3)_{mz} \\
&+ (\widetilde{D_0^x}v^1 + \widetilde{D_0^y}v^2 + \widetilde{D_0^z}v^3, \lambda(\widetilde{D_0^x}u^1 + \widetilde{D_0^y}u^2 + \widetilde{D_0^z}u^3))_h + (\widetilde{D_0^y}v^1 + \widetilde{D_0^x}v^2, \mu(\widetilde{D_0^y}u^1 + \widetilde{D_0^x}u^2))_h \\
&+ (\widetilde{D_0^z}v^1 + \widetilde{D_0^x}v^3, \mu(\widetilde{D_0^z}u^1 + \widetilde{D_0^x}u^3))_h + (\widetilde{D_0^z}v^2 + \widetilde{D_0^y}v^3, \mu(\widetilde{D_0^z}u^2 + \widetilde{D_0^y}u^3))_h.
\end{aligned} \tag{A.2}
$$

The term $R(\mathbf{v},\mathbf{u})$ is given by

$$
\begin{aligned}
R(\mathbf{v},\mathbf{u}) =& (D_+^x D_-^x v^1, \lambda D_+^x D_-^x u^1)_{rx} + (D_+^y D_-^y v^1, \mu D_+^y D_-^y u^1)_{ry} + (D_+^z D_-^z v^1, \mu D_+^z D_-^z u^1)_{rz} \\
&+ (D_+^x D_-^x v^2, \mu D_+^x D_-^x u^2)_{rx} + (D_+^y D_-^y v^2, \lambda D_+^y D_-^y u^2)_{ry} + (D_+^z D_-^z v^2, \mu D_+^z D_-^z u^2)_{rz} \\
&+ (D_+^x D_-^x v^3, \mu D_+^x D_-^x u^3)_{rx} + (D_+^y D_-^y v^3, \mu D_+^y D_-^y u^3)_{ry} + (D_+^z D_-^z v^3, \lambda D_+^z D_-^z u^3)_{rz}. \tag{A.3}
\end{aligned}
$$

We mention in passing that there is a typo in Eq. (A.9) in [20]. In that paper the $D_+^x D_-^x$, $D_+^y D_-^y$, and $D_+^z D_-^z$ operators were incorrectly given as $D_+^x D_+^x$, etc. The restricted scalar products are defined by

$$(u,v)_{mx} = h^3 \sum_{i=1}^{N_x-1} \sum_{j=1}^{N_y} \sum_{k=1}^{N_z} u_{i,j,k} v_{i,j,k}, \qquad (u,v)_{rx} = h^3 \sum_{i=2}^{N_x-1} \sum_{j=1}^{N_y} \sum_{k=1}^{N_z} u_{i,j,k} v_{i,j,k}$$

and $(u,v)_{my}$ is defined by a similar expression, but with the sum over i taken from 1 to N_x and the sum over j from 1 to N_y-1. In the same way, $(u,v)_{ry}$ has the sum over i taken from 1 to N_x and the sum over j from 2 to N_y-1. The sums in $(u,v)_{mz}$ and $(u,v)_{rz}$ are defined by corresponding permutations.

Note that both A and R are symmetric in their arguments. If $\mu > 0$ and $\lambda > 0$, all terms in $S^{(h)}(\mathbf{u},\mathbf{u})$ are non-negative, i.e., $S^{(h)}(\mathbf{u},\mathbf{u})$ is positive semi-definite. Finally, note that due to the restricted norms and the one-sided operators ($\widetilde{D_0^x}$ etc.) at the boundaries, no ghost points values are used in any of the terms in (A.2) and (A.3).

B The null-space of $S_\nu^{(h)}(\mathbf{u},\mathbf{u})$

In this section we discuss when $S_\nu^{(h)}(\mathbf{u},\mathbf{u})=0$. We simplify the notation of the vector components according to $\mathbf{u}=(u,v,w)^T$ and drop the ν-index on the material parameters λ and μ. Throughout the section we assume

$$\lambda \geq \lambda_{\min} > 0, \qquad \mu \geq \mu_{\min} > 0$$

at all grid points. By inspection of (A.1)-(A.3), we see that $S^{(h)}(\mathbf{u},\mathbf{u})$ is a sum of quadratic terms. Hence, $S^{(h)}(\mathbf{u},\mathbf{u})=0$ if and only if all terms are zero at each grid point. In order to make the term $R(\mathbf{u},\mathbf{u})=0$, all second divided differences of $\mathbf{u}$ must be zero at all grid points. Hence, $\mathbf{u}$ can only vary linearly in x, y and z.

The expression for $A(\mathbf{u},\mathbf{u})$ in (A.2) is a sum of seven non-negative terms. The only way $A(\mathbf{u},\mathbf{u})=0$ is if all seven terms in the sum are identically zero at all grid points. For all functions $\mathbf{u}$ that are linear in x, both $D_+^x\mathbf{u}$ and $\widetilde{D_0^x}\mathbf{u}$ are exact expressions of the x-derivative of $\mathbf{u}$. Since $\mathbf{u}$ is linear in all three coordinate directions, we can therefore replace all divided differences in by derivatives, and write the terms in $A(\mathbf{u},\mathbf{u})$ as

$$s_1=(u_x)^2, \quad s_2=(v_y)^2, \quad s_3=(w_z)^2, \quad s_4=(u_y+v_x)^2,$$
$$s_5=(u_z+w_x)^2, \quad s_6=(v_z+w_y)^2, \quad s_7=(u_x+v_y+w_z)^2.$$

If $s_1=s_2=s_3=0$, all terms in s_7 are also zero. Hence, there are only six independent conditions on $\mathbf{u}$ for making $S^{(h)}(\mathbf{u},\mathbf{u})=0$:

$$u_x=0, \qquad v_y=0, \qquad w_z=0, \tag{B.1}$$
$$u_y+v_x=0, \qquad u_z+w_x=0, \qquad v_z+w_y=0. \tag{B.2}$$

After some trivial compatibility arguments we arrive at the most general form of $f(y,z)$, $g(x,z)$, and $h(x,y)$ that satisfy (B.1), (B.2)

$$u(y,z)=f_0+yf_{y0}+zf_{z0}+yzf_{yz0}, \tag{B.3a}$$
$$v(x,z)=g_0+xg_{x0}+zg_{z0}+xzg_{xz0}, \tag{B.3b}$$
$$w(x,y)=h_0+xh_{x0}+yh_{y0}+xyh_{xy0}. \tag{B.3c}$$

Inserting (B.3a)-(B.3c) into (B.2) gives

$$f_{y0}+zf_{yz0}+g_{x0}+zg_{xz0}=0,$$
$$f_{z0}+yf_{yz0}+h_{x0}+yh_{xy0}=0,$$
$$g_{z0}+xg_{xz0}+h_{y0}+xh_{xy0}=0.$$

These expressions should be satisfied for any x, y, z. Taking $x=y=z=0$ gives

$$f_{y0}+g_{x0}=0, \qquad f_{z0}+h_{x0}=0, \qquad g_{z0}+h_{y0}=0. \tag{B.4}$$

Therefore,

$$f_{yz0}+g_{xz0}=0, \qquad f_{yz0}+h_{xy0}=0, \qquad g_{xz0}+h_{xy0}=0.$$

This non-singular linear system has the trivial solution $f_{yz0}=g_{xz0}=h_{xy0}=0$. Relation (B.4) provides three linear equations for $\mathbf{q}=(f_{y0},f_{z0},g_{x0},g_{z0},h_{x0},h_{y0})^T$,

$$C\mathbf{q}=0, \qquad C=\begin{pmatrix} 1 & 0 & 1 & 0 & 0 & 0 \\ 0 & 1 & 0 & 0 & 1 & 0 \\ 0 & 0 & 0 & 1 & 0 & 1 \end{pmatrix}.$$

Obviously, rank$(C)=3$. There are therefore three linearly independent non-trivial solutions of (B.4). In addition, the three undetermined constants f_0, g_0, and h_0 result in six linearly independent solutions of (B.1)-(B.2). They are often called the translational and rotational invariants, and can be written as

$$\begin{pmatrix} u \\ v \\ w \end{pmatrix} = \sum_{q=1}^{6} \alpha_q \mathbf{a}_q, \qquad \mathbf{a}_1 = \begin{pmatrix} 1 \\ 0 \\ 0 \end{pmatrix}, \qquad \mathbf{a}_2 = \begin{pmatrix} 0 \\ 1 \\ 0 \end{pmatrix}, \qquad \mathbf{a}_3 = \begin{pmatrix} 0 \\ 0 \\ 1 \end{pmatrix}, \qquad \text{(B.5)}$$

and

$$\mathbf{a}_4 = \begin{pmatrix} y \\ -x \\ 0 \end{pmatrix}, \qquad \mathbf{a}_5 = \begin{pmatrix} -z \\ 0 \\ x \end{pmatrix}, \qquad \mathbf{a}_6 = \begin{pmatrix} 0 \\ z \\ -y \end{pmatrix}. \qquad \text{(B.6)}$$

In summary, the null space for $S^{(h)}(\mathbf{u},\mathbf{u})$ has dimension six and is spanned by $\{\mathbf{a}_q\}_{q=1}^{6}$.

C   Proof of Lemma 4.1

Throughout this section, we simplify the notation by dropping the superscript (h) on the bilinear forms in (3.3) and denote $S_\nu^{(h)}$ and $B_\nu^{(h)}$ by S_ν and B_ν respectively. To reduce the amount of algebra, we assume $n=1$, and introduce the notation $\bar{\mathbf{u}}^{(1),m} = \bar{\mathbf{u}}^m$.

We start by writing (4.1) (for the case $n=1$) as

$$\rho \frac{\mathbf{u}^{m+1} - \mathbf{u}^m}{\Delta t^2} - \rho \frac{\mathbf{u}^m - \mathbf{u}^{m-1}}{\Delta t^2} = \mathbf{L}_h(\lambda_0,\mu_0)\mathbf{u}^m - \mathbf{L}_h(\lambda_1,\mu_1)\bar{\mathbf{u}}^m$$

and form the scalar product with $\mathbf{u}^{m+1} - \mathbf{u}^{m-1}$ to obtain

$$\left(\mathbf{u}^{m+1} - \mathbf{u}^{m-1}, \rho \frac{\mathbf{u}^{m+1} - \mathbf{u}^m}{\Delta t^2} - \rho \frac{\mathbf{u}^m - \mathbf{u}^{m-1}}{\Delta t^2} \right)_h$$
$$= (\mathbf{u}^{m+1} - \mathbf{u}^{m-1}, \mathbf{L}_h(\lambda_0,\mu_0)\mathbf{u}^m)_h - (\mathbf{u}^{m+1} - \mathbf{u}^{m-1}, \mathbf{L}_h(\lambda_1,\mu_1)\bar{\mathbf{u}}^m)_h.$$

For the left hand side, we write

$$\mathbf{u}^{m+1} - \mathbf{u}^{m-1} = (\mathbf{u}^{m+1} - \mathbf{u}^m) + (\mathbf{u}^m - \mathbf{u}^{m-1})$$

and use

$$(\mathbf{v}+\mathbf{w}, \mathbf{v}-\mathbf{w})_h = \|\mathbf{v}\|_h^2 - \|\mathbf{w}\|_h^2.$$

For the right hand side we use identity (3.3) on both terms. We obtain

$$\left\| \sqrt{\rho} \frac{\mathbf{u}^{m+1} - \mathbf{u}^m}{\Delta t} \right\|_h^2 - \left\| \sqrt{\rho} \frac{\mathbf{u}^m - \mathbf{u}^{m-1}}{\Delta t} \right\|_h^2$$
$$= -S_0(\mathbf{u}^{m+1} - \mathbf{u}^{m-1}, \mathbf{u}^m) + B_0(\mathbf{u}^{m+1} - \mathbf{u}^{m-1}, \mathbf{u}^m)$$
$$+ S_1(\mathbf{u}^{m+1} - \mathbf{u}^{m-1}, \bar{\mathbf{u}}^m) - B_1(\mathbf{u}^{m+1} - \mathbf{u}^{m-1}, \bar{\mathbf{u}}^m). \qquad \text{(C.1)}$$

The term $I_1 =: S_1(\mathbf{u}^{m+1} - \mathbf{u}^{m-1}, \bar{\mathbf{u}}^m)$ can be written

$$I_1 = S_1(\mathbf{u}^{m+1}, \bar{\mathbf{u}}^m) + S_1(\mathbf{u}^m, \bar{\mathbf{u}}^{m+1}) - S_1(\mathbf{u}^m, \bar{\mathbf{u}}^{m-1})$$
$$- S_1(\mathbf{u}^{m-1}, \bar{\mathbf{u}}^m) + S_1(\mathbf{u}^m, \bar{\mathbf{u}}^{m-1} - \bar{\mathbf{u}}^{m+1}).$$

By substituting (4.2) into the last term of I_1,

$$S_1(\mathbf{u}^m, \bar{\mathbf{u}}^{m-1} - \bar{\mathbf{u}}^{m+1}) = -\frac{1}{2\omega_1 \Delta t} S_1\left(\bar{\mathbf{u}}^{m+1} - \bar{\mathbf{u}}^{m-1}, \bar{\mathbf{u}}^{m+1} - \bar{\mathbf{u}}^{m-1}\right)$$
$$- \frac{1}{2} S_1\left(\bar{\mathbf{u}}^{m+1} + \bar{\mathbf{u}}^{m-1}, \bar{\mathbf{u}}^{m+1} - \bar{\mathbf{u}}^{m-1}\right)).$$

Since $S_1(\mathbf{u}, \mathbf{v}) = S_1(\mathbf{v}, \mathbf{u})$,

$$I_1 = S_1(\mathbf{u}^{m+1}, \bar{\mathbf{u}}^m) + S_1(\mathbf{u}^m, \bar{\mathbf{u}}^{m+1}) - S_1(\mathbf{u}^m, \bar{\mathbf{u}}^{m-1}) - S_1(\mathbf{u}^{m-1}, \bar{\mathbf{u}}^m)$$
$$- \frac{1}{2} S_1(\bar{\mathbf{u}}^{m+1}, \bar{\mathbf{u}}^{m+1}) + \frac{1}{2} S_1(\bar{\mathbf{u}}^{m-1}, \bar{\mathbf{u}}^{m-1}) - \frac{1}{2\omega_1 \Delta t} S_1\left(\bar{\mathbf{u}}^{m+1} - \bar{\mathbf{u}}^{m-1}, \bar{\mathbf{u}}^{m+1} - \bar{\mathbf{u}}^{m-1}\right).$$

Adding and subtracting $S_1(\bar{\mathbf{u}}^m, \bar{\mathbf{u}}^m)/2$ to I_1 and reorganizing the terms in (C.1) gives

$$e_1^{m+\frac{1}{2}} = e_1^{m-\frac{1}{2}} + B_0(\mathbf{u}^{m+1} - \mathbf{u}^{m-1}, \mathbf{u}^m) - B_1(\mathbf{u}^{m+1} - \mathbf{u}^{m-1}, \bar{\mathbf{u}}^m)$$
$$- \frac{1}{2\omega_1 \Delta t} S_1\left(\bar{\mathbf{u}}^{m+1} - \bar{\mathbf{u}}^{m-1}, \bar{\mathbf{u}}^{m+1} - \bar{\mathbf{u}}^{m-1}\right),$$

where

$$e_1^{m+\frac{1}{2}} = \left\|\sqrt{\rho}\frac{\mathbf{u}^{m+1} - \mathbf{u}^m}{\Delta t}\right\|_h^2 + S_0\left(\mathbf{u}^{m+1}, \mathbf{u}^m\right) - S_1\left(\mathbf{u}^{m+1}, \bar{\mathbf{u}}^m\right) - S_1\left(\mathbf{u}^m, \bar{\mathbf{u}}^{m+1}\right)$$
$$+ \frac{1}{2}\left[S_1\left(\bar{\mathbf{u}}^{m+1}, \bar{\mathbf{u}}^{m+1}\right) + S_1\left(\bar{\mathbf{u}}^m, \bar{\mathbf{u}}^m\right)\right].$$

This is equivalent to (4.3) for the case $n = 1$. The case $n \geq 2$ is treated analogously. For general $n \geq 1$, the expression for the discrete energy becomes

$$e^{m+\frac{1}{2}} = \left\|\sqrt{\rho}\frac{\mathbf{u}^{m+1} - \mathbf{u}^m}{\Delta t}\right\|_h^2 + S_0(\mathbf{u}^{m+1}, \mathbf{u}^m) - \sum_{\nu=1}^n \left(S_\nu(\mathbf{u}^{m+1}, \bar{\mathbf{u}}^{(\nu),m}) + S_\nu(\mathbf{u}^m, \bar{\mathbf{u}}^{(\nu),m+1})\right)$$
$$+ \frac{1}{2}\sum_{\nu=1}^n \left(S_\nu(\bar{\mathbf{u}}^{(\nu),m+1}, \bar{\mathbf{u}}^{(\nu),m+1}) + S_\nu(\bar{\mathbf{u}}^{(\nu),m}, \bar{\mathbf{u}}^{(\nu),m})\right). \tag{C.2}$$

By expanding all quadratic terms in (4.4) it is straight forward to verify that it is equivalent to (C.2). This concludes the proof of Lemma 4.1.

References

[1] K. Aki and P. G. Richards, Quantitative Seismology, University Science Books, Sausalito, CA, USA, 2nd edition, 2002.

[2] R. J. Apsel and J. E. Luco, On the green's functions for a layered half-space, Bull. Seismol. Soc. Am., 73 (1983), 931–951.

[3] J. Bielak, H. Karaoglu and R. Taborda, Efficient simulation of anelastic wave propagation by the octree-based finite element method-an improved approach, Seismol. Res. Lett., 81 (2010), 321. Seismological Society of America, 2010.

[4] J. M. Carcione, Wave fields in real media: wave propagation in anisotropic, anelastic and porous media, volume 31 of Handbook of Geophysical Exploration: Seismic Exploration, Pergamon, Elsevier Science, 2001.

[5] S. M. Day, J. Bielak, D. Dreger, S. Larsen, R. Graves, A. Pitarka and K. B. Olsen, Test of 3D elastodynamic codes: Lifelines program task 1A02, Technical report, Pacific Earthquake Engineering Center, 2003.

[6] S. M. Day and C. Bradley, Memory-efficient simulation of anelastic wave propagation, Bull. Seismol. Soc. Am., 91 (2001), 520–531.

[7] S. M. Day and J. B. Minister, Numerical simulation of attenuated wavefields using a Padé approximant method, Geophys. J. R. Astr. Soc., 78 (1984), 105–118.

[8] H. Emmerich and M. Korn, Incorporation of attenuation into time-dependent computations of seismic wave fields, Geophysics, 52(9) (1987), 1252–1264.

[9] V. D. Glushenkov, A difference analog of the Korn inequality, J. Soviet Math., 46 (1989), 2176–2182.

[10] R. W. Graves and S. M. Day, Stability and accuracy analysis of coarse-grain viscoelastic simulations, Bull. Seismol. Soc. Am., 93(1) (2003), 283–300.

[11] C. O. Horgan, Korn's inequalities and their applications in continuum mechanics, SIAM Rev., 37 (1995), 491–511.

[12] M. Käser, M. Dumbser, J. de la Puente and H. Igel, An arbitrary high-order discontinuous Galerkin method for elastic waves on unstructured meshes-III: viscoelastic attenuation, Geophys. J. Int., 168 (2007), 224–242.

[13] D. Komatitsch, Q. Liu, J. Tromp, P. Süss, C. Stidham and J. H. Shaw, Simulations of ground motion in the Los Angeles basin based upon the spectral-element method, Bull. Seismol. Soc. Am., 94(1) (2004), 187–206.

[14] D. Komatitsch and J. Tromp, Introduction to the spectral element method for three-dimensional seismic wave propagation, Geophys. J. Int., 139 (1999), 806–822.

[15] J. Kristek and P. Moczo, Seismic-wave propagation in viscoelastic media with material discontinuities: a 3D fourth-order staggered-grid finite-difference modeling, Bull. Seismol. Soc. Am., 93(5) (2003), 2273–2280.

[16] H.-P. Liu, D. L. Anderson and H. Kanamori, Velocity dispersion due to anelasticity, implications for seismology and mantle composition, Geophys. J. R. Astr. Soc., 47 (1976), 41–58.

[17] P. Liu and R. J. Archuleta, Efficient modeling of Q for 3D numerical simulation of wave propagation, Bull. Seismol. Soc. Am., 96 (2006), 1352–1358.

[18] P. Moczo and J. Kristek, On the rheological models used for time-domain methods of seismic wave propagation, Geophys. Res. Lett., 32 (2005), L01306.

[19] S. Nilsson, N. A. Petersson, B. Sjögreen and H.-O. Kreiss, Stable difference approximations for the elastic wave equation in second order formulation, SIAM J. Numer. Anal., 45 (2007), 1902–1936.

[20] N. A. Petersson and B. Sjögreen, An energy absorbing far-field boundary condition for the elastic wave equation, Commun. Comput. Phys., 6 (2009), 483–508.

[21] N. A. Petersson and B. Sjögreen, User's guide to WPP version 2.1. Technical report LLNL-SM-487431, Lawrence Livermore National Laboratory, 2011. (Source code available from `https://computation.llnl.gov/casc/serpentine`).

[22] N. A. Petersson and B. Sjögreen, Stable grid refinement and singular source discretization for seismic wave simulations, Commun. Comput. Phys., 8(5) (2010), 1074–1110.

[23] B. Savage, D. Komatitsch and J. Tromp, Effects of 3D attenuation on seismic wave amplitude and phase measurments, Bull. Seismol. Soc. Am., 100(3) (2010), 1241–1251.

[24] J. Virieux, *P-SV* wave propagation in heterogeneous media: velocity-stress finite-difference method, Geophysics, 51(4) (1986), 889–901.

[25] L. Zhu, The frequency-wavenumber (FK) synthetic seismogram package, available at `http://www.eas.slu.edu/People/LZhu/home.html`, 1999.

[26] L. Zhu and L. A. Rivera, A note on the dynamic and static displacements from a point source in multilayered media, Geophys. J. Int., 148 (2002), 619–627.